STATISTICS OF MET-OCEAN CONDITIONS BETWEEN WEST AND CENTRAL GULF OF MEXICO BASED ON FIELD MEASUREMENTS

A Thesis

by

LIN SU

Submitted to the Office of Graduate Studies of
Texas A&M University
in partial fulfillment of the requirements for the degree of

MASTER OF SCIENCE

May 2012

Major Subject: Civil Engineering

Statistics of Met-ocean Conditions between West and Central Gulf of Mexico Based on Field Measurements

STATISTICS OF MET-OCEAN CONDITIONS BETWEEN WEST AND CENTRAL GULF OF MEXICO BASED ON FIELD MEASUREMENTS

A Thesis

by

LIN SU

Submitted to the Office of Graduate Studies of
Texas A&M University
in partial fulfillment of the requirements for the degree of

MASTER OF SCIENCE

Approved by:

Chair of Committee,	Jun Zhang
Committee Members,	Hamn-Ching Chen
	Benchun Duan
Head of Department,	John Niedzwecki

May 2012

Major Subject: Civil Engineering

ABSTRACT

Statistics of Met-Ocean Conditions between West and Central Gulf of Mexico Based on Field Measurements. (May 2012)

Lin Su, B.S., Hohai University

Chair of Advisory Committee: Dr. Jun Zhang

Statistics of met-ocean conditions including wind, current and wave at the location between west and central Gulf of Mexico (GOM) are derived based on about three year of field measurements. Two-parameter Weibull distribution has been employed to fit wind speed at 10m over sea level and current speed in various depth. The joint probability contour was derived based on First-Order Reliability Method. In addition, the joint distribution of wind speed and direction was visualized by wind-rose diagram. The results provided in this study may provide essential information to the probability distribution of met-ocean condition in the particular location and can be used as a reference in the future designs.

ACKNOWLEDGEMENTS

I would like to express my deep gratitude to my committee chair, Dr. Zhang, under whose general supervision this study could finally carry out. Thanks so much to my committee members, Dr. Chen and Dr. Duan, for their keen guidance and support throughout the course of this research.

Thanks also to my friends and colleagues and the department faculty and staff for making my time at Texas A&M University a great experience. Thanks to Chengxi Li for providing pivot work on wind data validation and thanks to Chao Zhou for his kind help in MATLAB programming. I also want to extend my gratitude to Adam Kiecke and Anadarko Petroleum Company for providing the data.

Finally, thanks to my mother and father for their encouragement and to my wife for her great patience and love.

NOMENCLATURE

NDBC	National Data Buoy Center
API	American Petroleum Institute
APC	Anadarko Petroleum Institute
BMT	British Maritime Technology
EPRMS	Environment and Platform Response Monitoring System
GOM	Gulf of Mexico
GPS	Global Positioning System
RP	Recommended Practice
PDF	Probability Density Function
CDF	Cumulative Distribution Function
Hs	Significant Wave Height
Tp	Peak Period
FORM	First-Order Reliability Method
6DoF	Six Degree of Freedom

TABLE OF CONTENTS

Page

LIST OF FIGURES

Page

LIST OF TABLES

Page

1. INTRODUCTION

The Constitution Truss Spar operated by Anadarko Petroleum Corporation (APC), is located in Green Canyon Block 679 and 680 in a water depth of 5,000 ft. That is, it is located in the API transition zone between the West and Central Gulf of Mexico. The SPAR was installed in October of 2006 and has since weathered multiple hurricanes and storms. Right after its installation, British Maritime Technology (BMT) installed an Environmental Platform Response Monitoring System (EPRMS). The EPRMS is an integrated system collecting myriad of data that include the magnitude and direction of current and wind, one-hour average significant wave height and peak period at the location of the TRUSS SPAR, its six-degree of freedom (6DoF) motions, and tensions in its mooring lines and Top-Tension Risers. With the permission from APC, these data are available to the Ocean Engineering Program at Texas A&M University. This study intended to derive the statistics and probability distributions of wind，current and wave based upon 35 months measurements recorded at the SPAR, including joint distribution of significant wave height and peak period, wind speed distribution, wind rose plots, etc. Efforts have also been made on seeking the relationship. The results obtained from this

This thesis follows the style of Ocean Engineering.

study may provide essential information pertaining to the probability distributions of met-ocean conditions that can be used in designing the offshore structures located in API transition zone.

For Wind speed distribution, two-parameter Weibull distribution has widely been examined in many cases worldwide. Rehman et al. (1994) used two-parameter Weibull distribution to fit the yearly wind speed data of several coastal cities in Saudi Arabic. Three methods: the maximum likelihood method, the proposed modified maximum likelihood method and the graphical method for calculating the parameters of two-parameter Weibull wind speed distribution for wind energy analysis are presented by Seguro and Lambert (2000). Jaramillo (2004) fitted the annual and seasonal wind speed data of La Ventosa, Mexico by Weibull distribution. Jowder (2006) applied two-parameter Weibull distribution to wind data measured at Bahrain International airport from 2003 to 2005. Monahan (2006) analyzed daily sea winds observations measured by scatterometer in a global region and pointed out that the two-parameter Weibull distribution always gave a good approximation (but not the perfect) to the sea wind speed probability density function.

2. DATA DESCRIPTION AND COMPARISON

The APC EPRMS collects data at a 4Hz sampling rate, and records over 130 channels of raw environment and platform response data. The data available to us is within the period from June 2007 to April 2010. A detailed description of this type of monitoring system and its advantages can be found in Prislin, et al. (2005) and Irani, et al. (2007). All data is appropriately filtered, translated, analyzed and quality controlled before release by BMT. The EPRMS data used for this study are as follows:

- Hourly average 6DoF motions of the Spar
- Hourly average significant wave height and peak period
- Hourly average surface and maximum current magnitude and direction
- Hourly average Wind speed and direction

Due to the routine maintenance and occasional malfunction of certain instruments, it is necessary to remove part of the data that are obviously erroneous and not applicable for further analysis. For instance, a minus 9999 always indicated that the data is not available. We can simply identify the inaccurate data if the same value repeated in a dataset for a suspiciously long period. To make sure the remaining data is reliable, the comparison with related NOAA data and Navy Archive data in the nearby region have been made. The basic idea for data verification is to ensure the EPRMS is working

properly based on the comparison with nearby measurements. The comparison cannot verify whether or not the EPRMS data is accurate considering the large distance between the sites of measurements. The comparison may validate the data if the comparing sets show the similar trend. If the EPRMS data has the same trend with the nearby site, we are convinced that EPRMS data is reliable. It should be noticed that the wind speed and direction can stay similar in a relatively large range which enables us to choose the sites for wind data verification in a larger area than that in case of current, because the current speed and direction can always be altered by many factors such as loopcurrent.

2.1 Wind Data

The speed and direction of winds during a storm are crucial in the design of offshore structures because of the large force they can apply on the offshore structure. Wind speed during a hurricane conditions in the Gulf of Mexico (GOM) can, for example, reach over 150 km/h causing 450 KN or more horizontal forces on a typical offshore structure (Dyrbye and Hansen, 1997). The hourly average wind speed and direction have been recorded during the three years, including several extreme weather conditions such as, hurricane Ike on September 12, 2008, when the recorded wind speed exceeded 40 m/s. Following the meteorological convention of wind direction, when the wind blowing from the north direction its direction is defined as zero degree and the degree clockwise

increased. In our study, the EPRMS wind direction data follows the meteorological convention as shown in Fig.1. For example, the wind comes from the east would be counted as 90 degree. The wind data of Constitution is recorded by two anemometers respectively, one on the crane and the other on the flareboom. It is understood that the crane and platform heading might change with time. Due to the complexity of crane data transformation, the data from the flare boom was used in this study. The flareboom for Constitution Spar is a 185ft long structure, fixed at an angle of 60 degree to the topside.

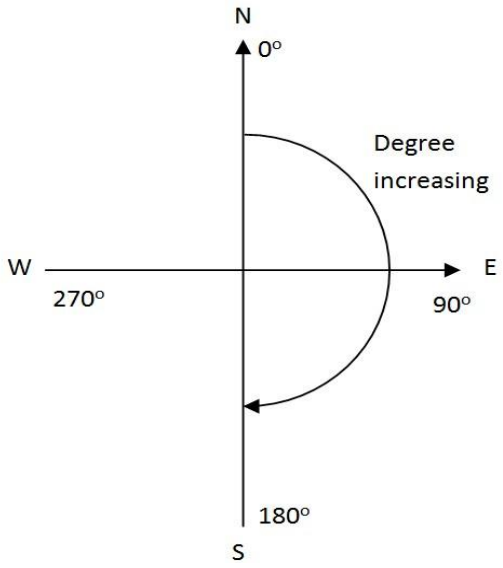

Fig. 1 Illustration of wind direction recording convention

To ensure the validity of the wind data, the related data from National Data Buoy Center, Station 42897 is chosen to conduct wind velocity comparison. The selected site

is located at 89°51'36" West Longitude and 27°19'52" North Latitude about 80 kilometers on the east side of the Constitution. We randomly selected the wind data of two-day period (Feb.4 2008 ~ Feb.5 2008) for the comparison of wind velocity in both direction and magnitude. As the anemometer for Station 42897 is set 5 meters above the sea level, a translation to a standard wind velocity at 10 meter above the sea level was made following API (American Petroleum Institute) rule for wind. That is, the wind speed varies with height above the sea surface.

$$\bar{U}(z) = \bar{U}_{ref}\left(z / z_{ref}\right)^{a} \qquad (1)$$

where z is the elevation above the mean water level, the reference elevation z_{ref} =10m and the mean speed at the reference elevation is $\overline{U}_{ref}$. The over bar of U denotes a time-average. The exponential index a is equal to 0.125. The transformation of EPRMS wind data has also been performed accordingly.

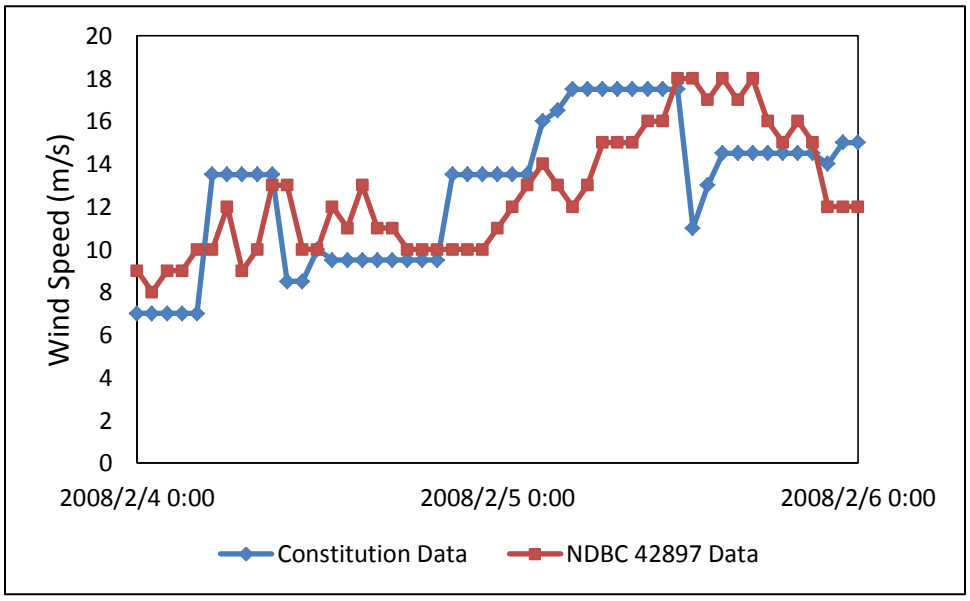

Fig. 2 Wind direction comparison with NOAA data

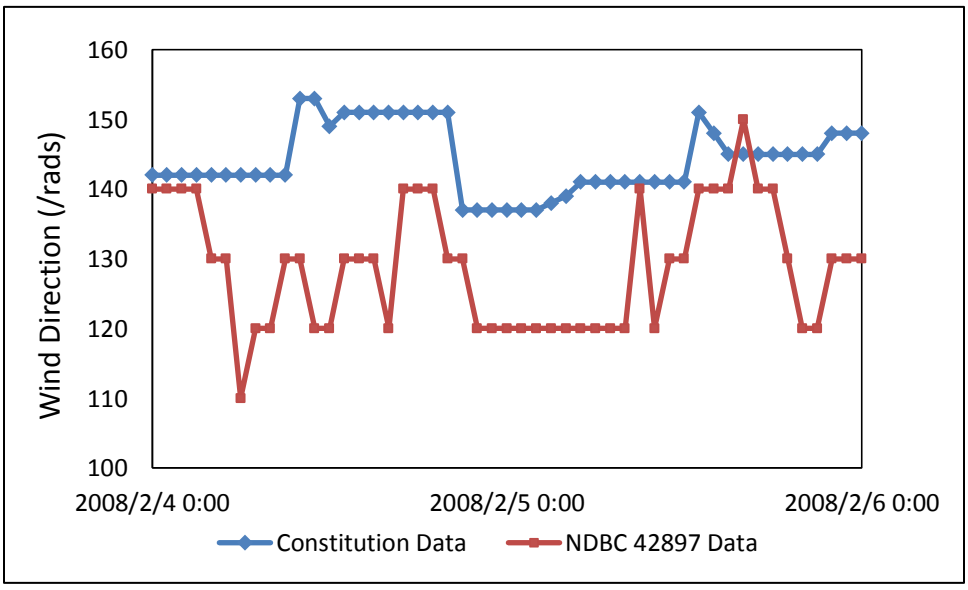

Fig. 3 Wind speed comparison with NOAA data

The comparisons of wind speed and direction between EPRMS field data and NOAA data are given in Fig.2 and Fig.3, respectively. The overall agreement shown in the two figures are good. The difference in direction is roughly within 30 degree and the speed keeps very close.

2.2 Current Data

Ocean currents are normally driven by density, pressure and temperature gradients. The EPRMS data provide current speeds and directions for surface current and current with maximum velocity which is also of great significance to the SPAR response analysis. For validation, the surface current data recorded by EPRMS has been compared with Navy Archive Data and NDBC Station 42886. The current direction data was recorded in an opposite way from wind direction mentioned in Section 2.1. When the current flow towards the true north, its direction is defined as zero degree and the degree clockwise increased.

The Naval Archive Data presents the daily-average current speed and direction, namely, only one figure for each day. The colors in the figure indicate different current speeds according to the color bar attached and the black trend line with arrow indicates the current direction. Due to the lower resolution of naval archive data, the comparison of surface current direction cannot be performed accurately. Therefore, the scheme for

the surface current data comparison is to randomly select several current speed data from both groups of high current speed and relatively low current speed after sorting the data by speed. Then we can make the comparison by picking up the navy archive data in these certain days at the location of Constitution SPAR at 90° 58' 4.8" West Longitude and 27° 17' 31.9" North Latitude.

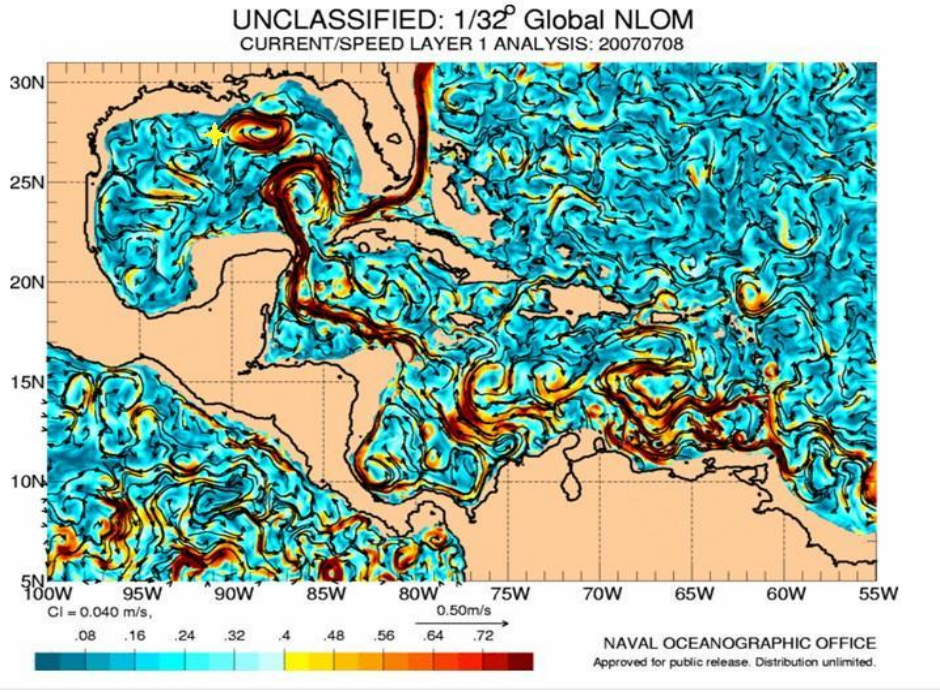

Fig. 4 The comparison of deep current speed with navy archive data on July 08, 2007 (http://www7320.nrlssc.navy.mil/global_nlom32/navo/IASSP1/TOPEX+ERS2+GFO+MOD_SP1_IASSP1_20070708.001.gif)

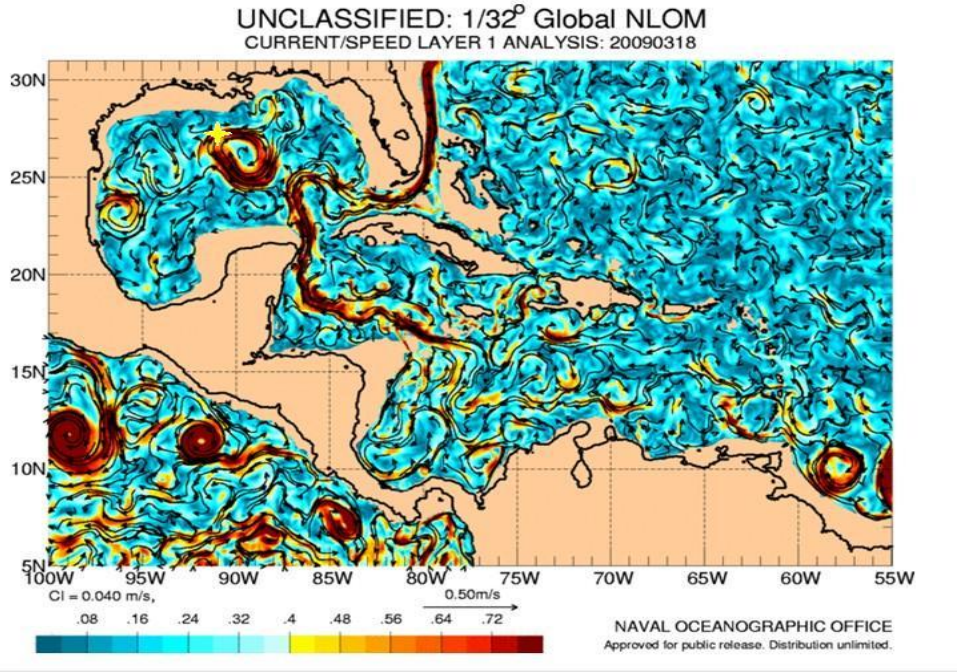

Fig. 5 The comparison of surface current speed with naval archive data on March 18, 2009 (http://www7320.nrlssc.navy.mil/global_nlom32/navo/IASSP1/TOPEX+ERS2+GFO+MOD_SP1_IASSP1_20090318.001.gif)

In Fig.4, Constitution Spar marked by the highlighted star is located almost on the edge of the new eddy of the loop current in Gulf of Mexico (GOM). The current speed reached over 0.3m/s which is in good agreement with the daily average 0.28m/s of the EPRMS measurements on July 8, 2007. Similarly, the EPRMS data shows that on March 18, 2009 the surface current speed exceeded 0.8m/s when loop current shifted to the SPAR location as shown in Fig. 5. Since the comparison shows good agreement of the sets of data, we consider the EPRMS data is reliable.

Current speeds at surface have been also compared with the nearby NDBC station 42886--Discoverer Spirit, an mobile offshore drilling unit operated by Anadarko Petroleum Corporation which is located at 90°50'11" West Longitude and 27°13'24" North Latitude about 10 kilometers on the southeast of Constitution Spar. The data from midnight of Jan 9th, 2009 to midnight of Jan 13th were chosen for current speed comparison near the surface. The current data recorded at NDBC Station 42886 was at 62.5m depth and below. Thus we chose the current speed at 62.5m depth for comparison. It is shown that the data from two sites have good agreement in trend but different magnitudes. We may conclude that both measurements were working properly. However, it is very suspicious that the current speed for NDBC Station 42886 at 62.5m depth was much larger than that of surface current for EPRMS data as shown in Fig.6.

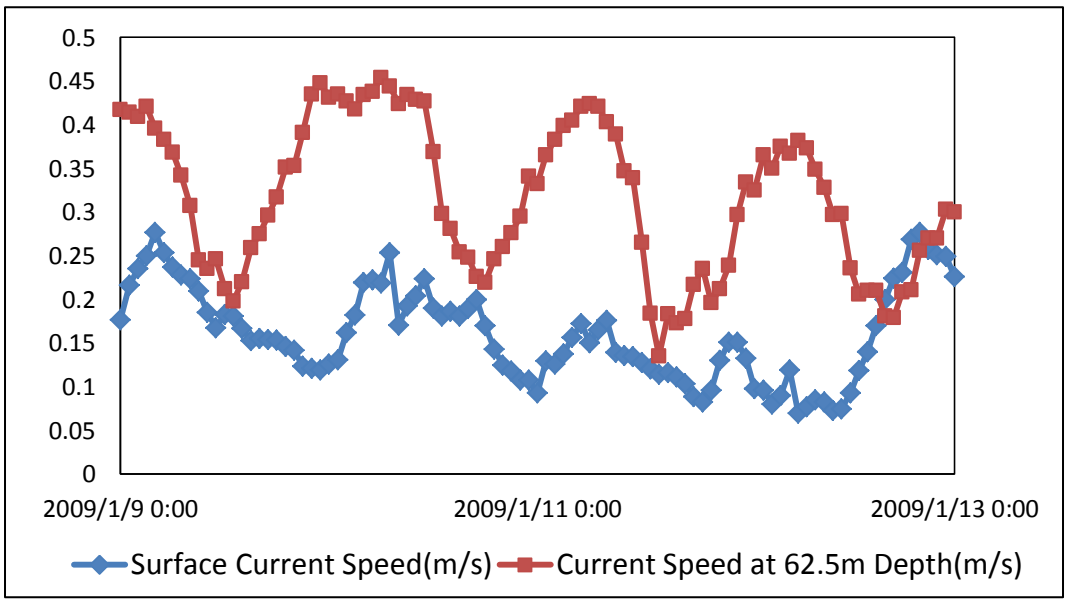

Fig. 6 Surface current comparison between NDBC Station 42886 and Constitution Spar

It is found that the so-called maximum current speed in EPRMS data is not always larger than the surface current as shown in Fig.7. The number in x-axis indicates how many hours have been counted since the sampling period for EPRMS current speed is one hour. We cannot distinguish which data has measurement problem or even both of them are not reliable. In that case, even though the surface current comparison has positive result, we have to choose the data from NDBC Station 42886 for the further current speed statistics since the EPRMS data is suspicious to some extent.

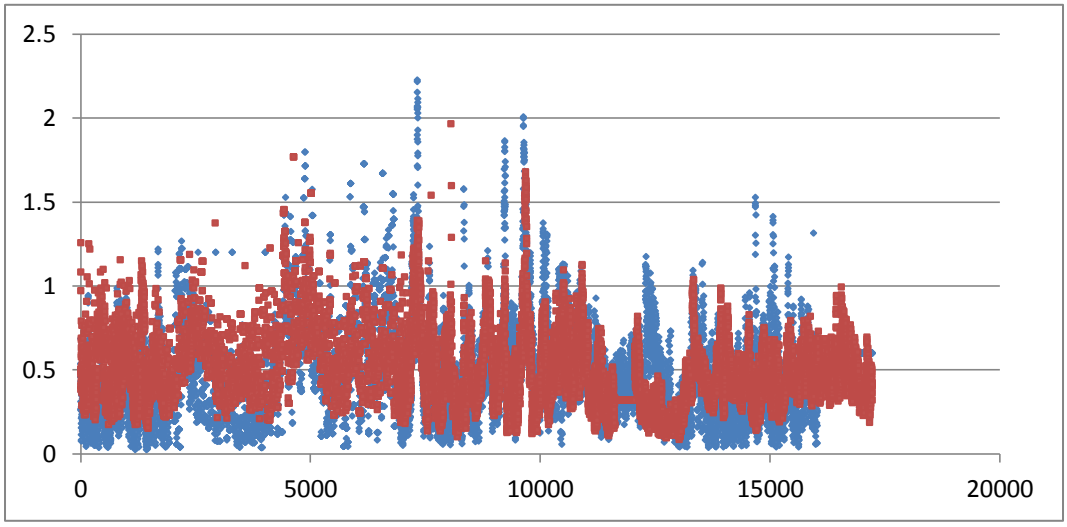

Fig. 7 The comparison between surface current speed and maximum current speed for EPRMS data

2.3 Wave Data

Unfortunately, the wave data is currently unavailable on the nearby NBDC site. The nearest NDBC Station 42041- North Mid Gulf about 110 nautical miles (NM) of South Grand Isle was disestablished on March 16, 2005. Three nearest NDBC Stations were chosen for the comparison as shown in Fig.8. Station 42001 was known as Station of Central Gulf of Mexico and located at 89° 67' West Longitude and 25° 86' North Latitude, which is about 200 kilometers southeast from Constitution SPAR. Station 42002 was known as Station of Western Gulf of Mexico and located at 93° 66' West Longitude and 25° 79' North Latitude, and Station 42040 located at 88° 12' West Longitude and 29° 17' North Latitude on the northeast of Constitution SPAR.

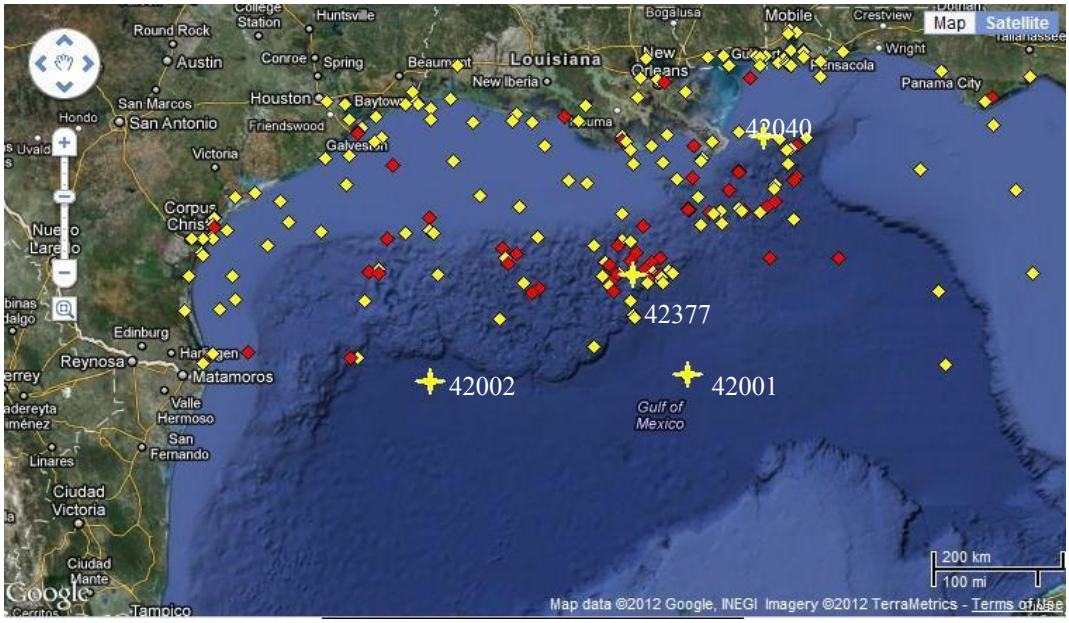

Fig. 8 The location of three NDBC station 42001, 42002, 42040 and the Constitution SPAR 42377 (http://www.ndbc.noaa.gov/)

The available data of these three Stations are only standard meteorological data including significant wave height (Hs), Dominant wave period and Average wave period. Significant wave height (meters) is for the duration of 10-minute sampling period, while the EPRMS significant wave height is for the duration of an hour. The comparison has been done in randomly selected continuous four days duration starting from the midnight of January 1st to the midnight of January 5th, 2009. Based on the comparison shown in Fig.9 we noticed that the data of Station 42001 and 42002 have the great similarity in significant wave height magnitude, however the data from Station 42040 shows more difference in comparison with the EPRMS data. It is not surprising

that the EPRMS data does not closely match the magnitude with either of the two stations 42001 and 42002 since they were far apart from Constitution. However, they show the same trend of variation in the significant wave height as represented in Fig.9.

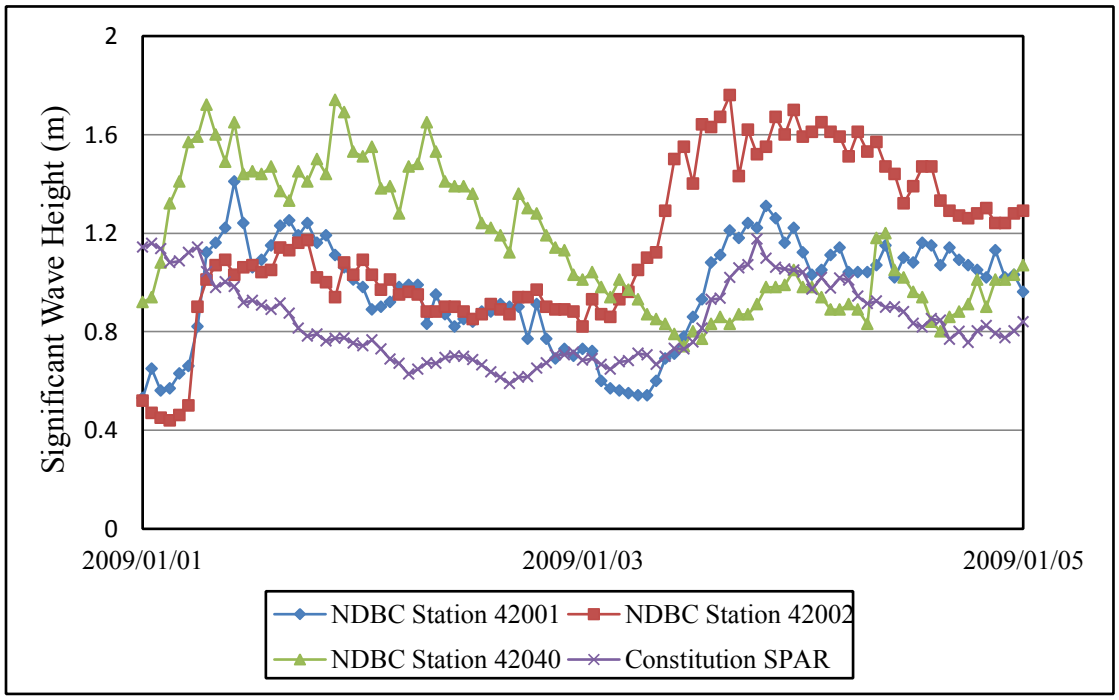

Fig. 9 The comparison of significant wave height between the EPRMS data and the NDBC Station 42001, 42002 and 42040 data

We compared the corresponding wave peak period from Jan 1st to Jan 5th. Except for the data from Station 42002, the Constitution data, 42001 data and 42040 data matched well as shown in Fig.10. Especially in the middle of Jan 3th, an obvious decreasing in peak period was observed in the trend lines of Station 42001 and Constitution Spar (They are also the two closest among the four sites). Due to the far distance between the

four stations, more accurate results of comparison in significant wave height and peak period are not available.

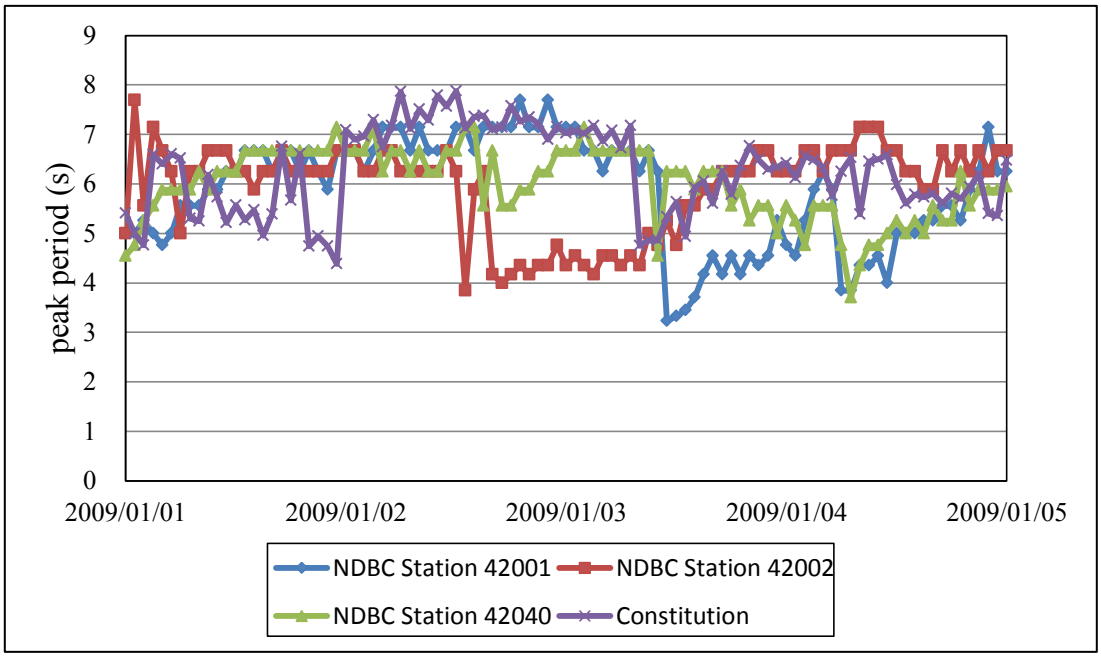

Fig. 10 Comparison for peak period between the EPRMS data and the NDBC Station 42001, 42002 and 42040 data

3. STATISTICS OF MET-OCEAN CONDITIONS

Wind, current and ocean wave are crucial to the design and safety of offshore structures. Many studies were made to explore the monthly, seasonal and yearly probability distribution of wind speed. Jaramillo (2004), Jowder (2006) and Monahan (2006) used two-parameter Weibull distribution in wind speed fitting in various sites worldwide. We followed their methods to show the statistics and probability of wind. Wind-rose diagrams were plotted to reveal the joint distribution of wind speed and direction. The probability distribution of current speed for three depths from upper to lower (62.4m, 154.4m and 258.4m) were obtained following the same method used in the case of wind. The joint probability contour of significant wave height and peak period was also derived following the method of Winterstein et al. (1993) based on the First Order Reliability Method (FORM).

3.1 Wind Speed Distribution

We have the EPRMS hourly-average wind speed and direction data for the duration of 35 months. However, it should be noticed that in 2008 the data from May 1st to July 30th were excluded mainly for the malfunction of the sensors. In addition, the related data from September 2009 and January 2010 are also incomplete. Therefore the

available data are for 30 months except for sporadic missing data. If 30 days for one month is assumed, there should be 24*30=720 data for each month. For example, there are only 543 hourly-average wind speed data in December 2009 less than the average data number because there is no data after Christmas which caused a loss of data (7*24=168 counts).

A two-factor Weibull distribution is used to model the wind speed distribution. It describes the probability density of wind speed above a given value x is determined by

$$f\left(x|a,b\right)=ba^{-b}x^{b-1}exp\left[-\left(x/a\right)^{b}\right] \qquad (2)$$

where b is the gust parameter and a the scale parameter and x the hourly wind speed. All of them are in unit of meters per second. The two parameters a and b are estimated using a maximum log-likelihood method. The maximum log-likelihood method is intended to find the unique estimations of parameters by pursuing a maximum joint probability density for the given variable. Therefore the observations we obtained must have the greatest joint probability density when the best fitting distribution with proper parameters are given. The Weibull negative log-likelihood for uncensored data is

$$\left(-\ln L\right)=-\ln\prod_{i=1}f\left(x_i|a,b\right)=-\sum_{i=1}^{n}\ln f\left(x_i|a,b\right) \qquad (3)$$

,

where the continued product of Weibull probability density function is denoted by L. Taking the logarithm of the L when the hourly-average wind speeds and Eqn.(2) are satisfied,

$$-\ln L = -\ln\left[\left(1/a^b\right)^n b^n \left(\prod_{i=1}^{n} x_i^{b-1} \right) exp(-1/a^b \sum_{i=1}^{n} x_i^b) \right] \qquad (4)$$

Eqn.(4) is the expansion of negative log-likelihood of Weibull probability density function. The maximum value of –lnL can be reached, when Eqn.(5) is satisfied.

$$\begin{cases} \partial \ln L/\partial b = -n\ln a + n/b + \sum_{i=1}^{n} \ln x_i - 1/a^b \sum_{i=1}^{n} x_i^b \ln x_i + 1/a^b \left(\ln a\right) \sum_{i=1}^{n} x_i^b = 0 \\ \partial \ln L/\partial a = -nb/a + b/a^{b+1} \sum_{i=1}^{n} x_i^b = 0 \end{cases} \qquad (5)$$

After algebraic manipulation, Eqn.(5) can be simplified as,

$$\begin{cases} 1/b + 1/n \sum_{i=1}^{n} \ln x_i - 1 \Big/ \sum_{i=1}^{n} x_i^b \sum_{i=1}^{n} x_i^b \ln x_i = 0 \\ a = \left(1/n \sum_{i=1}^{n} x_i^b \right)^{b^{-1}} \end{cases} \qquad (6)$$

Eqn.(6) is a set of nonlinear equations and an iteration method is used to obtain the numerical solution. The results and figures provided here can be obtained using the function wblfit which can be found in distribution fitting tool (dfittool) in MATLAB Statistics toolbox. The function wblfit provides the estimations of scale parameter a and

gust parameter b based on the maximum likelihood theory introduced earlier. In this study, Input variable for function wblfit is the hourly-average wind speed.

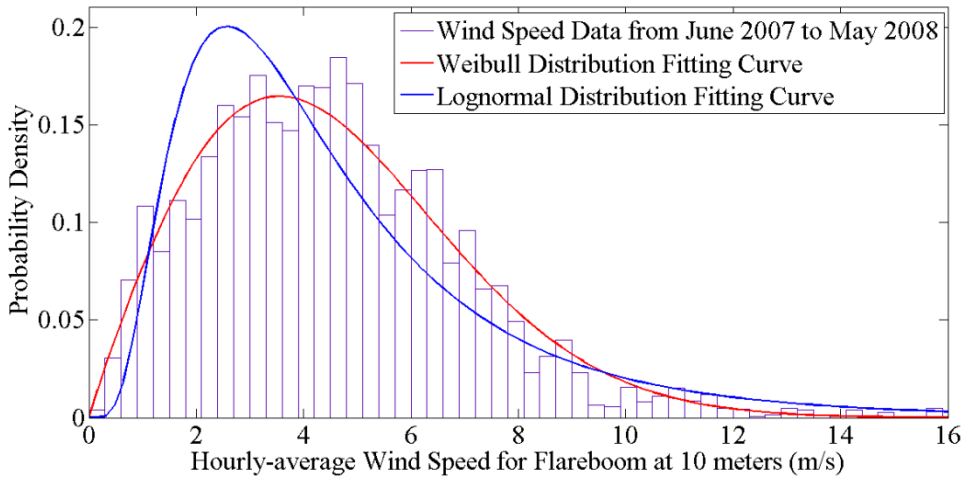

Fig. 11 Weibull probability density function for data from June 2007 to May 2008

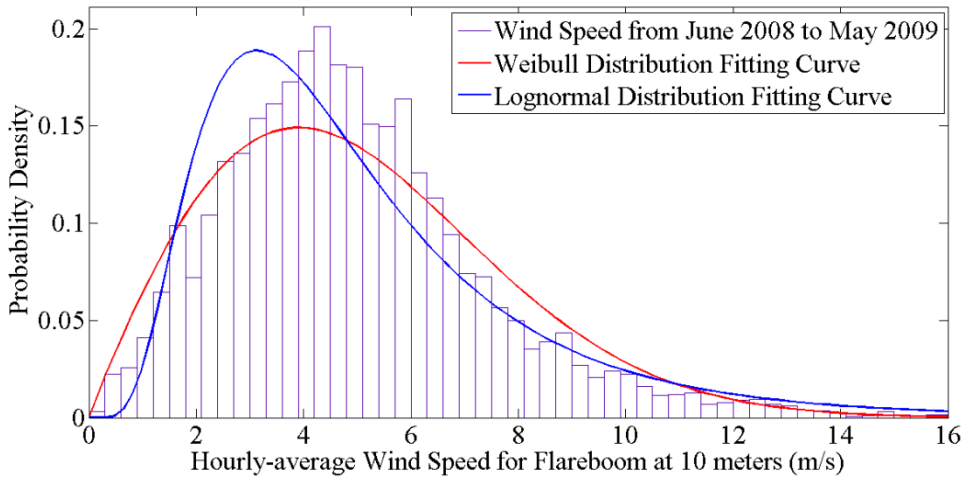

Fig. 12 Weibull probability density function for data from June 2008 to May 2009

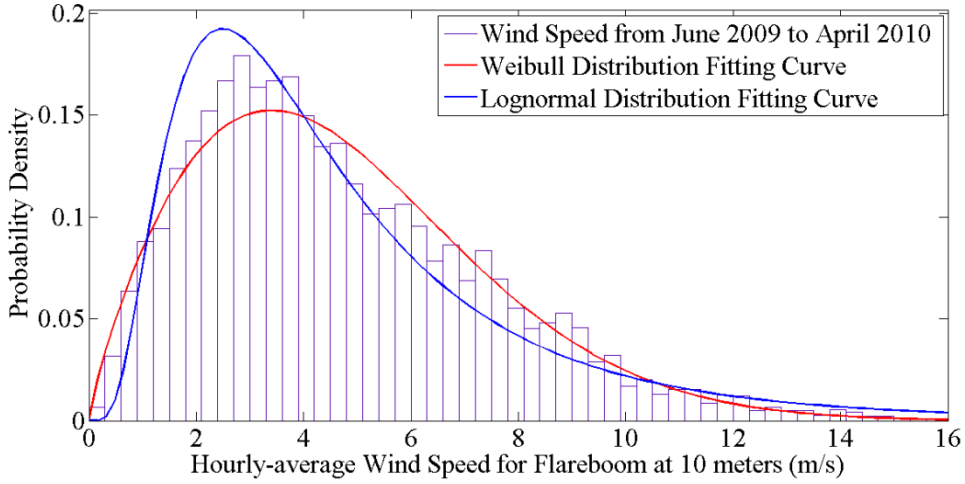

Fig. 13 Weibull probability density function for data from June 2009 to April 2010

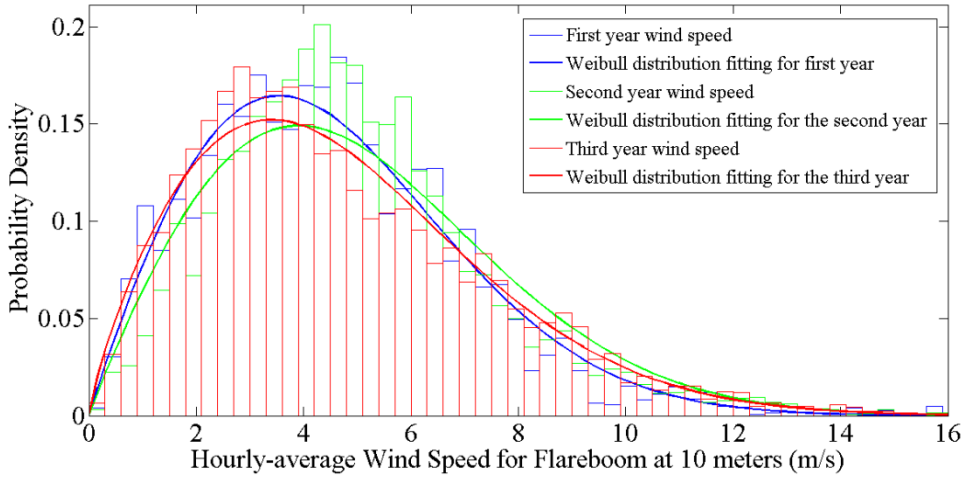

Fig. 14 the three year Weibull fitting comparison

The comparison between Weibull Distribution and Lognormal Distribution Fittings has been made in Fig.11, Fig.12 and Fig.13. It is clear that the Weibull Distribution has the better agreement with measured data. In Fig.14, the three year wind speed distribution have the similar pattern with small differences in both scale parameter a and

gust parameter b. Table 1 reveals that the mean value of wind speed varies little during the three-year period, ranging from 5.127 to 5.655m/s. The second year has the largest mean wind speed with the scale parameter a equal to 5.655m/s. It might be caused by the effects of great numbers of the large storms occurred in 2008, such as hurricane Ike. But the loss of data in May, June, July 2008 may also have an important impact on the value of the mean wind speed. It can be found that the mean wind speed kept very small during the summer that is June, July and August. The great loss of wind speed data in months with small wind speed partially explain why the large mean value of wind speed occurred in the second year in comparison with the other two years results. In Fig.13, we can see wind speed distribution in the third year is getting closer to the lognormal distribution in comparison with the first two years. It is because that in the third year the probability density bars for wind speed ranging from 4m/s to 6m/s denoted by red color are much lower than other two years as shown in Fig.14. We should notice that there are two months' data unavailable in the third year in Table 2, September 2009 and January 2010 which have large mean wind speed around 5m/s for both months based on the data of the other two years. The gust parameter b is ranging from 1.81 to 1.95 which indicates that the fitted two-parameter Weibull distribution is very close to its special case, the Rayleigh distribution when gust parameter is equal to 2.

Table 1

Detailed statistical results for three year wind speed Weibull distribution

Statistical results	The 1st year's wind speed	The 2nd year's wind speed	The 3rd year's wind speed
Number of available data	7766	6771	6118
Mean (m/s)	4.547	5.014	4.714
Median (m/s)	4.830	5.225	4.640
Maximum (m/s)	19.374	42.263	18.109
Minimum (m/s)	0.105	0.099	0.148
a (Scale Parameter)	5.127	5.655	5.302
b (Gust parameter)	1.950	1.949	1.809
Weibull distribution	$Y=0.081X^{0.95}\ exp[-(X/5.13)^{1.95}]$	$Y=0.066X^{0.95}exp[-(X/5.67)^{1.95}]$	$Y=0.088X^{0.81}exp[-(X/5.302)^{1.81}]$

Table 2

The details for monthly wind Weibull distribution estimations of parameters

	Counts	Average Wind Speed(m/s)	a(Scale Parameter)	b(Gust parameter)
June 2007	587	3.83	4.33	2.11
July 2007	741	3.00	3.38	1.83
August 2007	728	3.56	4.00	1.75
September 2007	720	4.74	5.38	1.98
October 2007	742	5.49	6.18	2.58
November 2007	720	3.98	4.48	1.90
December 2007	744	4.28	4.83	1.88
January 2008	636	5.67	6.37	2.73
February 2008	690	5.37	6.06	2.26
March 2008	739	6.01	6.79	2.07
April 2008	713	5.21	5.83	2.99
August 2008	627	3.71	4.19	2.02
September 2008	678	5.54	6.08	1.40
October 2008	743	4.42	4.98	2.36
November 2008	719	4.56	5.14	2.02
December 2008	740	5.44	6.65	2.05
January 2009	686	4.67	5.27	2.05
February 2009	672	5.06	5.68	2.76
March 2009	744	5.62	6.32	2.65
April 2009	719	6.34	7.15	2.48
May 2009	397	4.49	5.03	3.06
June 2009	719	3.41	3.85	2.23
July 2009	742	3.06	3.45	2.56
August 2009	738	2.50	2.82	2.07
October 2009	741	4.92	5.56	2.39
November 2009	604	5.27	5.95	1.96
December 2009	543	6.19	6.99	2.18
February 2010	592	5.99	6.76	2.28
March 2010	719	6.05	6.83	1.95
April 2010	720	5.69	6.42	2.40

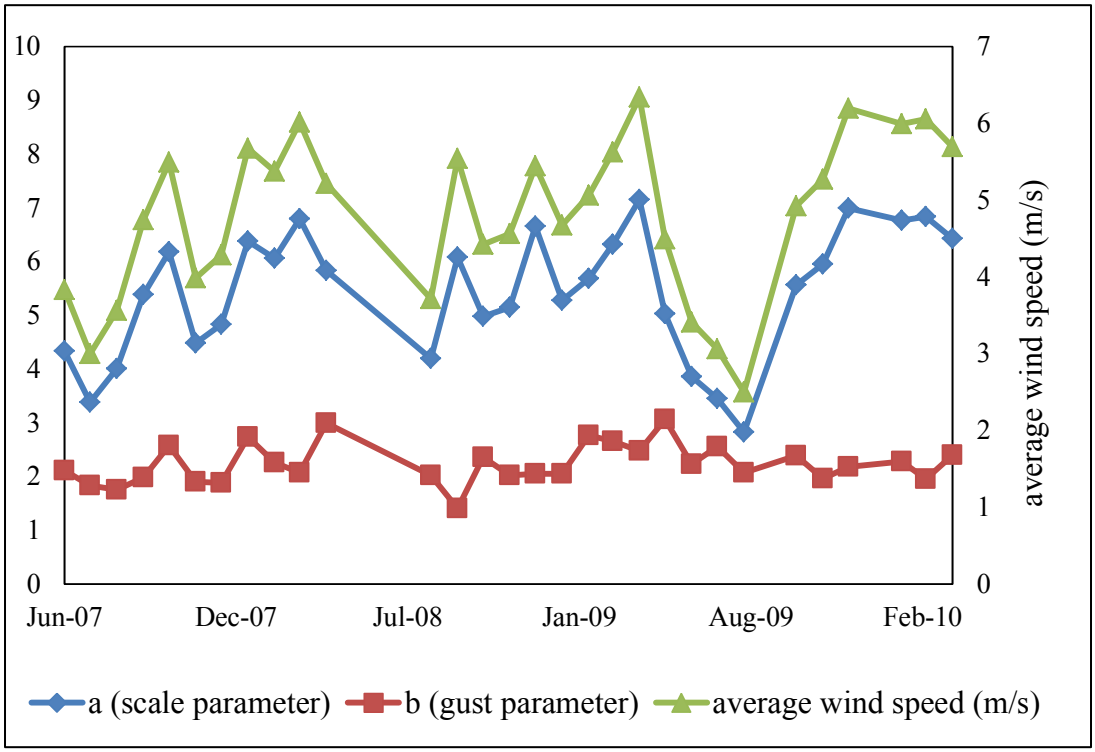

Fig. 15 The variation of scale parameter a and gust parameter b and the average wind speed for three-month period

Table 2 shows that the average wind speed was smallest in summer from June to August and gradually increased during fall and winter, and reached the maximum in spring from March to May during the period of June 2007 to May 2008. The three years data in general followed this pattern as shown in Fig.15. The scale parameter a in Weibull distribution is proportional to the average wind speed and the gust parameter b has large value when the mean wind speed is large. This observation is expected because the increase in mean wind speed by hurricanes or sea storms often leads to great

fluctuation in wind speed. The mean of parameter a is 5.43 and the mean of parameter b is 2.11. The maximum wind speed occurred in 9/12/2008 with a magnitude of 44.16 m/s when Hurricane Ike passing nearby and the mean wind speed during 9/11/2008-9/12/2008 is 16.58 m/s. All figures for monthly wind speed distribution are given in Appendix A, while the Weibull distribution parameters for each month are listed in Table 2.

3.2 Wind Rose Diagram

The rose diagrams of wind velocity were plotted to reveal both direction and magnitude. The four quadrants were divided into thirty-six sectors, namely, ten degree for each sector. The radius of each sector indicates how many times that wind was blowing to within the defined 10-degree range and also the segments within each sector distinguished by different colors indicate the speed magnitude in the same sector. The length of each segment is proportional to its overall percentage in the sector. In wind rose diagram, the mean wind speed is at 10 meters above the sea surface and the unit is m/s. The direction of wind rose diagram follows the rule of current direction we mentioned in Chapter 2, that is, the recorded degree indicates the direction that current flows to.

Fig.16 shows the wind-rose diagram in different season based on 35 months data from June 2007 to April 2010. The wind data of several months (May-June 2008, September 2009 and January 2010) were missing or partially unavailable. The upper-left wind-rose diagram (a) was made by collecting wind speed and direction data from all March-to-May periods during 35 months and the upper-right diagram (b) is from June to August. Similarly, the lower-left (c) one is from September to November and the lower-right (d) is for December to February. As we can see in the Fig.16, the main trend for wind direction at the location of Constitution is northwest and southwest. During the season of spring (see (a)), about 50 percent of wind is blowing to the northeast direction. However the largest wind speed occurs when wind blows to southeast direction during the spring. The diagram (d) shows that the largest wind speed for winter occurs in the fourth quadrant blowing to the south-east. There is no clear pattern for the summer wind diagram (b) because the direction is widely-spread and the magnitude of wind velocity is the smallest among the four seasons. The largest wind speed distinctly increases (reach 35m/s, the actual largest hourly-average wind speed is not collected because of the missing of its direction) for the autumn mainly due to the Hurricane Ike in Sep, 2008. The mean wind speed for autumn is similar to the spring but direction shifts to the southwest. After the overview of the wind-rose diagram, we can basically conclude that the sway motion of the platform (translation in west-east direction) should be taken into

consideration since the wind dominant direction is towards the west. It should be noticed that the maximum wind speed would not only occurred towards west. The wind at sea surface in north hemisphere would converge counter-clockwisely to the hurricane eye during a hurricane. Therefore considering the relative position of Constitution Spar and the path of hurricane, the direction of largest wind could have great diversity.

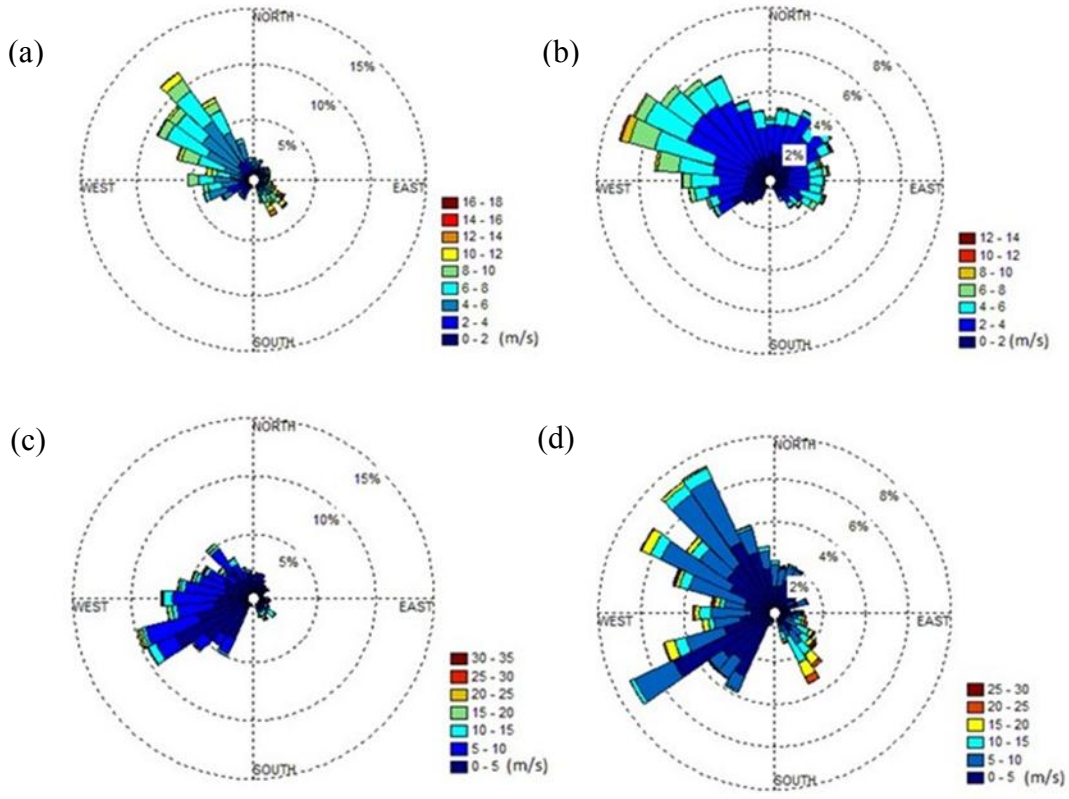

Fig. 16 Three year wind rose diagrams in spring, summer, autumn and winter based on 35 months measurements. (a) the wind rose diagram for spring from March to May; (b) the wind rose diagram for Summer from June to August; (c) the wind rose diagram for fall from September to November; (d) the wind rose diagram for winter from December to February

3.3 Current Speed and Direction

Current data from NDBC Station 42886 were adopted for current statistics for the same duration as EPRMS data. Unfortunately, the current data of NDBC Station 42886 are not available in the second half of year 2007 but the data in 2008 and 2009 are basically intact. First, we examined the data in time history to see if their distribution is varying by depth. As shown in Fig.17, the current speeds at four depths (62.5m, 126.3m, 190.5m and 254.5m) have good agreement and also decrease in magnitude with the increase in depth which observes the physical law known as Ekman Layer. It should be noticed that the data in September 2008 is partially missing. Therefore we can see sparse dots widespread during that month and the current statistics given below does not include the data for this month.

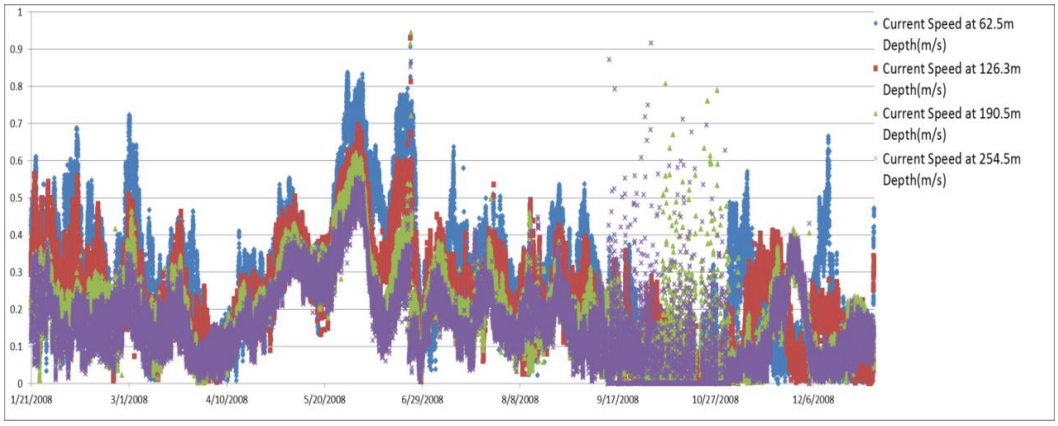

Fig. 17 Current speed comparison at different depth for NDBC Station 42886 during 2008

The current speed statistics started from the February 2008 and ended on Dec 2009. Monthly and yearly distributions of current speed at 62.4m, 158.4m and 254.4m depth were derived following the same methods described in the previous section of analyzing, namely, using two-parameter Weibull distribution fitting. Three tables (Tables 3-5) given below contain detailed parameters for current Weibull distribution at the three different depths. We can find that the trends in time history for current mean value and scale parameter a are in good agreement and the magnitude decrease with the increase in the depth. The maximum average current speed occurred usually during the February and March for each year which is quite similar to the wind distribution pattern. Since the surface current is highly related to the wind at sea surface, it is a very convincible sign that can correlate the wind data. The minimum current speed always occurred in November and December, which does not agree with the wind statistics. All figures for monthly current speed distribution at three depths (62.4m, 158.4m and 254.4m) can be found in Appendix B.

Table 3

The details for monthly current Weibull distribution estimations of parameters at 62.4m depth

Current at 62.4m depth	Counts	Mean (m/s)	a(Scale Parameter)	b(Shape Parameter)
Feb 2008	701	0.358	0.397	3.593
Mar 2008	377	0.297	0.335	2.021
Apr 2008	413	0.165	0.184	1.618
May 2008	738	0.298	0.331	3.377
Jun 2008	590	0.576	0.636	3.968
Jul 2008	716	0.307	0.344	2.946
Aug 2008	674	0.275	0.308	3.177
Oct 2008	688	0.076	0.080	1.119
Nov 2008	444	0.160	0.164	1.076
Dec 2008	710	0.200	0.224	1.704
Jan 2009	563	0.299	0.338	2.206
Feb 2009	665	0.560	0.618	3.937
Mar 2009	658	0.377	0.424	2.789
Apr 2009	604	0.233	0.263	2.121
May 2009	591	0.172	0.187	1.311
Jun 2009	706	0.168	0.190	2.196
Jul 2009	717	0.201	0.225	2.809
Aug 2009	722	0.148	0.167	2.635
Sep 2009	707	0.257	0.288	1.633
Oct 2009	616	0.224	0.248	3.629
Nov 2009	248	0.142	0.159	1.985
Dec 2009	673	0.119	0.130	1.409

Table 4

The details for monthly current Weibull distribution estimations of parameters at 158.4m depth

Current Speed at 158.4m Depth	Counts	Mean (m/s)	a(Scale Parameter)	b(Shape Parameter)
Feb 2008	701	0.237	0.263	3.646
Mar 2008	377	0.203	0.228	2.664
Apr 2008	413	0.112	0.126	1.662
May 2008	738	0.270	0.299	3.829
Jun 2008	590	0.411	0.460	3.168
Jul 2008	716	0.224	0.249	3.631
Aug 2008	674	0.183	0.205	3.003
Oct 2008	688	0.068	0.075	1.360
Nov 2008	444	0.090	0.093	1.098
Dec 2008	710	0.153	0.171	1.609
Jan 2009	563	0.194	0.218	3.077
Feb 2009	665	0.337	0.378	2.923
Mar 2009	658	0.270	0.297	4.303
Apr 2009	604	0.195	0.220	2.453
May 2009	591	0.144	0.158	1.404
Jun 2009	706	0.108	0.121	2.972
Jul 2009	717	0.164	0.185	2.429
Aug 2009	722	0.118	0.133	1.763
Sep 2009	707	0.231	0.256	1.501
Oct 2009	616	0.105	0.107	1.033
Nov 2009	248	0.104	0.117	2.175
Dec 2009	673	0.073	0.082	1.743

Table 5

The details for monthly current Weibull distribution estimations of parameters at 254.4m depth

Current Speed at 254.4m Depth	Counts	Mean (m/s)	a(Scale Parameter)	b(Shape Parameter)
Feb 2008	701	0.164	0.184	2.852
Mar 2008	377	0.163	0.182	2.913
Apr 2008	413	0.100	0.113	1.860
May 2008	738	0.238	0.264	3.610
Jun 2008	590	0.315	0.356	2.402
Jul 2008	716	0.173	0.193	3.015
Aug 2008	674	0.161	0.181	2.671
Oct 2008	688	0.117	0.125	1.230
Nov 2008	444	0.081	0.089	1.352
Dec 2008	710	0.145	0.161	1.490
Jan 2009	563	0.153	0.172	3.319
Feb 2009	665	0.228	0.257	2.721
Mar 2009	658	0.209	0.232	3.570
Apr 2009	604	0.131	0.148	2.026
May 2009	591	0.115	0.127	1.489
Jun 2009	706	0.094	0.105	3.005
Jul 2009	717	0.123	0.138	2.602
Aug 2009	722	0.093	0.100	1.238
Sep 2009	707	0.238	0.264	1.547
Nov 2009	248	0.073	0.082	1.806
Dec 2009	673	0.069	0.078	1.812

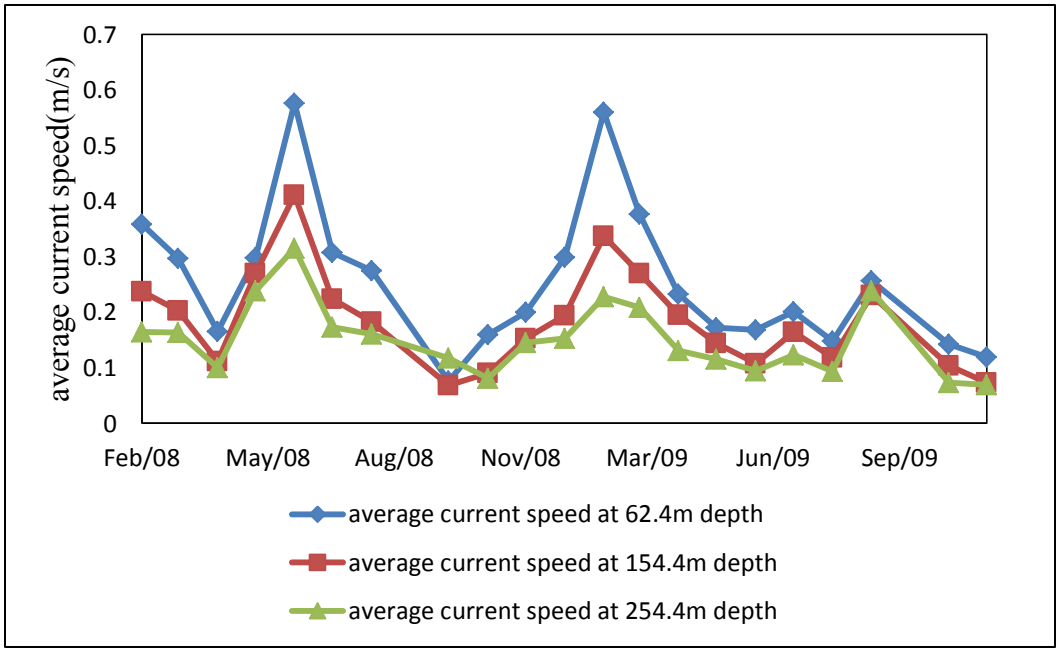

Fig. 18 Comparison between average current speed in three depths during 2008 and 2009

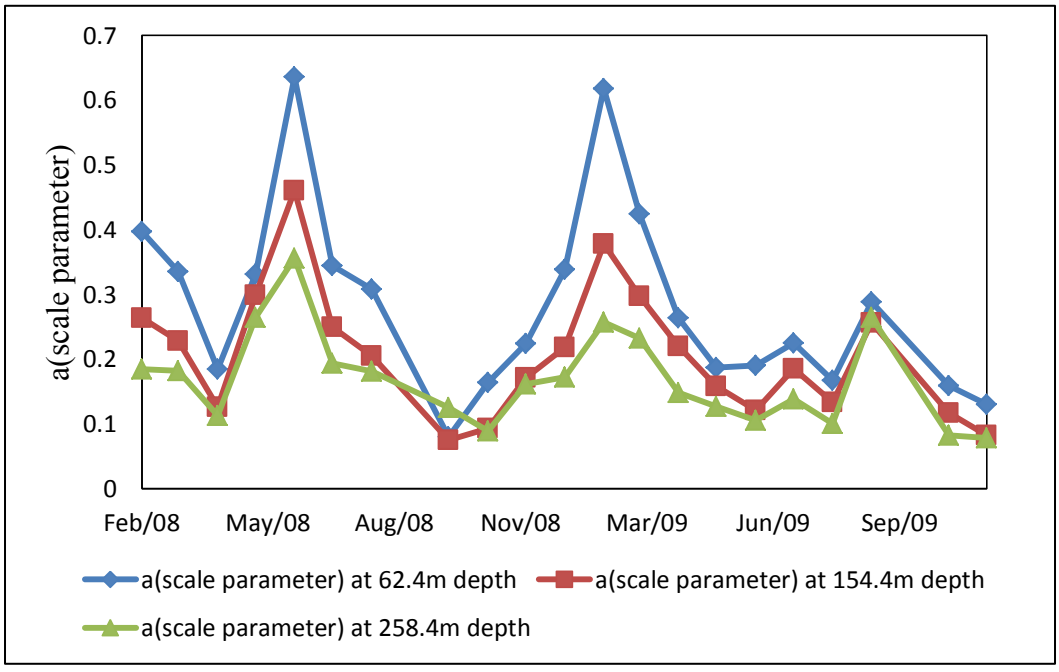

Fig. 19 Comparison between scale parameter a in three depths during 2008 and 2009

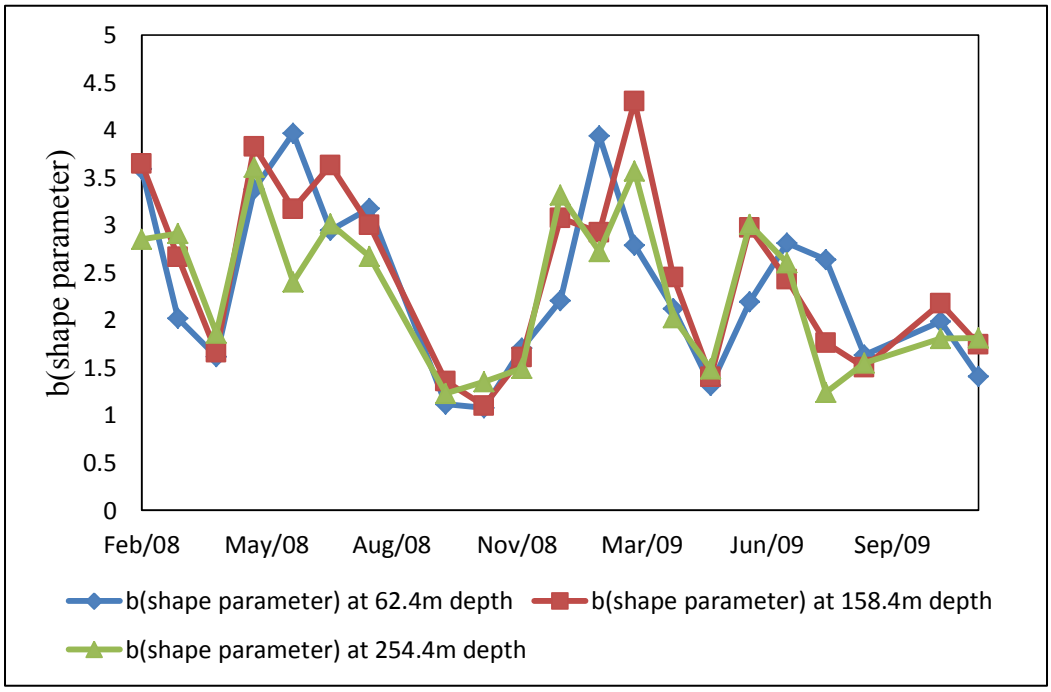

Fig. 20 Comparison between shape parameter b in three depths during 2008 and 2009

All the statistical results from Table 3 to Table 5 were also plotted in Figures 18-20, which compare the average current speed, scale parameter a and shape parameter b at the three different depths. As we mentioned before, the average current speed is highly correlated with the scale parameter. Therefore, it is not surprising that their trends in time are virtually the same. There are no obvious seasonal pattern for average current speed and scale parameter a. It is known that the maximum value can be reached when the loop-current occurred nearby. The magnitude for average current speed and scale parameter a at different depths have larger differences when loop-current occurred and keep close to each other when the average current speeds are relatively low. The

variation of shape parameter b in different depths basically follow the trend same as the scale parameter a. It usually reached the maximum when the current speed was large.

We can also see that the mean current speed during June 2008 was quite unusual. It was very strong reaching 0.576 m/s in comparison with the data in June 2009 (0.168m/s) which is thought to be very small during the summer as well as wind data. Therefore the Naval Archive data were employed for data checking during June 2008 as shown in Fig.21. We choose the daily-average surface current results from June 5th to June 30th with a 5-day interval which can basically demonstrate the current variation during June 2008. The NDBC Station 46882 is marked by the highlighted triangle which is located almost the same position as Constitution Spar. During June 2008, the location of NDBC Station 42886 mostly overlapped the dark red region indicating 0.72 m/s.

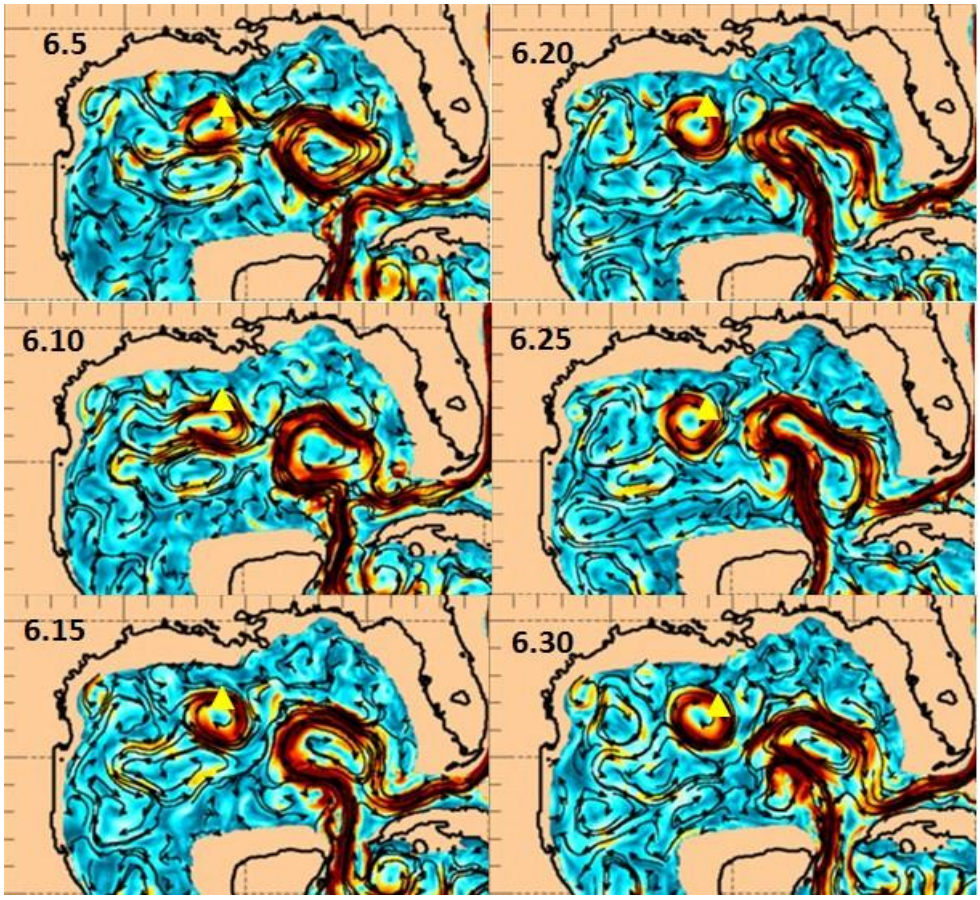

Fig. 21 Surface current condition during June 2008 at the location of NDBC Station 42886

On the contrary, the mean current speed is quite small during June 2009 as shown in Table 3. Although it seems reasonable as we noticed from the dataset (Wind and current are usually very small in summer), to find out the reason for difference between current data in June 2008 and 2009, we use the Naval Archive data again for comparison in 2009 as shown in Fig.22. Surprisingly, we find that the NDBC Station 42886 was very close to the edge of existed loop-current eddy. However, it was always located at the dark blue region, namely, the region with very low current speed according to the color

bar we mentioned in Chapter 2. It is always true that the wind over sea surface has a great contribution to the surface current speed by momentum exchange. However, the current speed also reaches a higher level in some month without large wind speed such as June 2008 we illustrated before. Based on the statistics results for now we can conclude that the current speed on the upper layers (above 250m depth) in GOM is mainly relative to the loop-current.

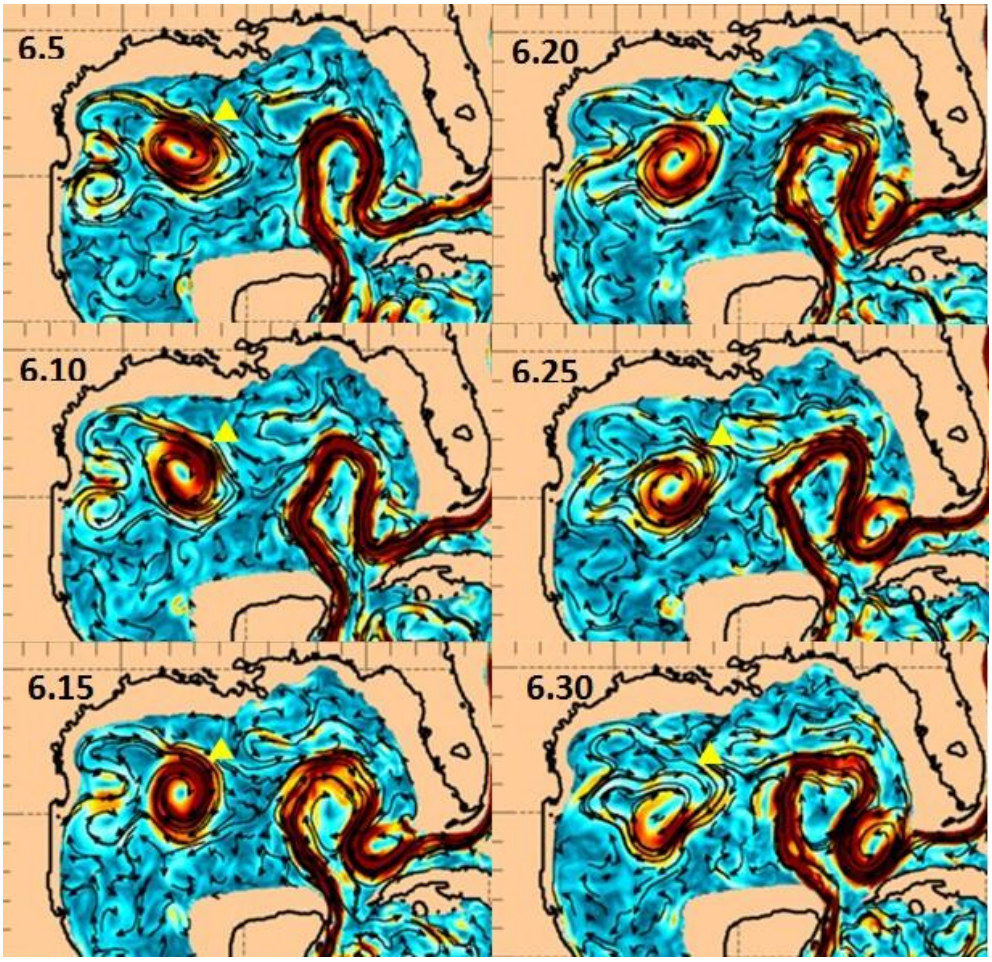

Fig. 22 Surface current condition during June 2009 at the location of NDBC Station 42886

The yearly current speed distributions in three depths have also been derived and shown from Fig.23 to Fig.28. The yearly data is well fitted by the Weibull distribution and both scale parameter a and shape parameter b are similar for 2008 and 2009.

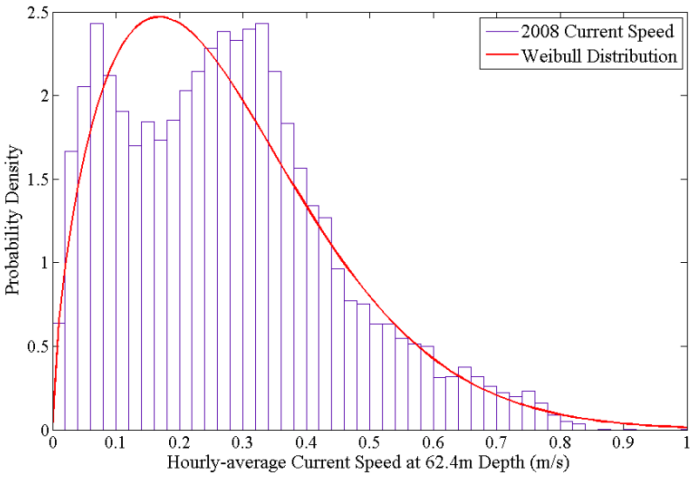

Fig. 23 Current speed distribution and Weibull fitting at 62.4m for 2008

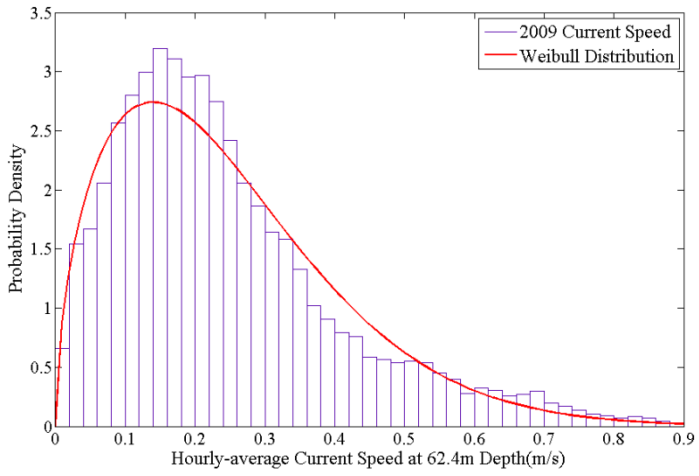

Fig. 24 Current speed distribution and Weibull fitting at 62.4m for 2009

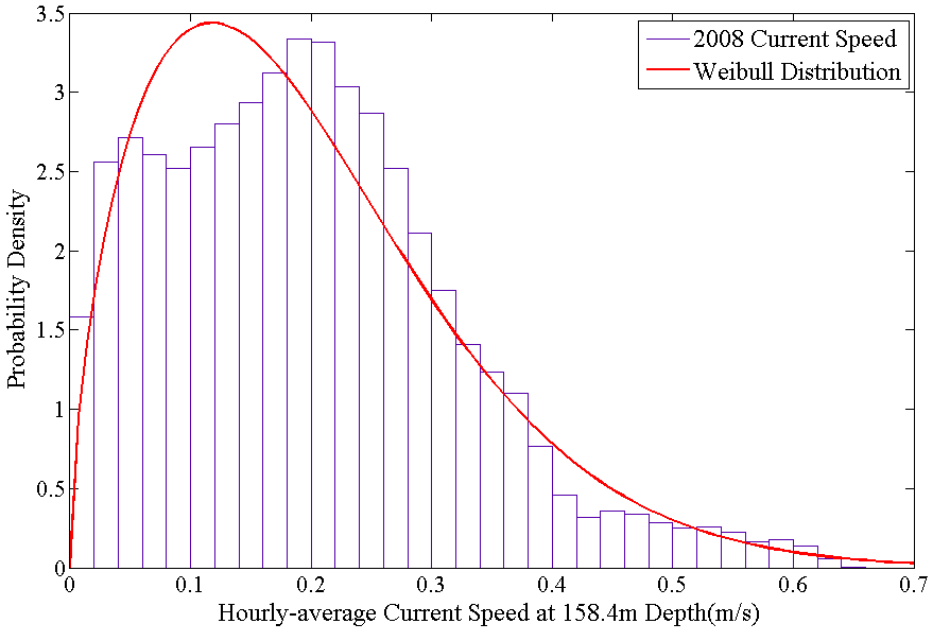

Fig. 25 Current speed distribution and Weibull fitting at 158m for 2008

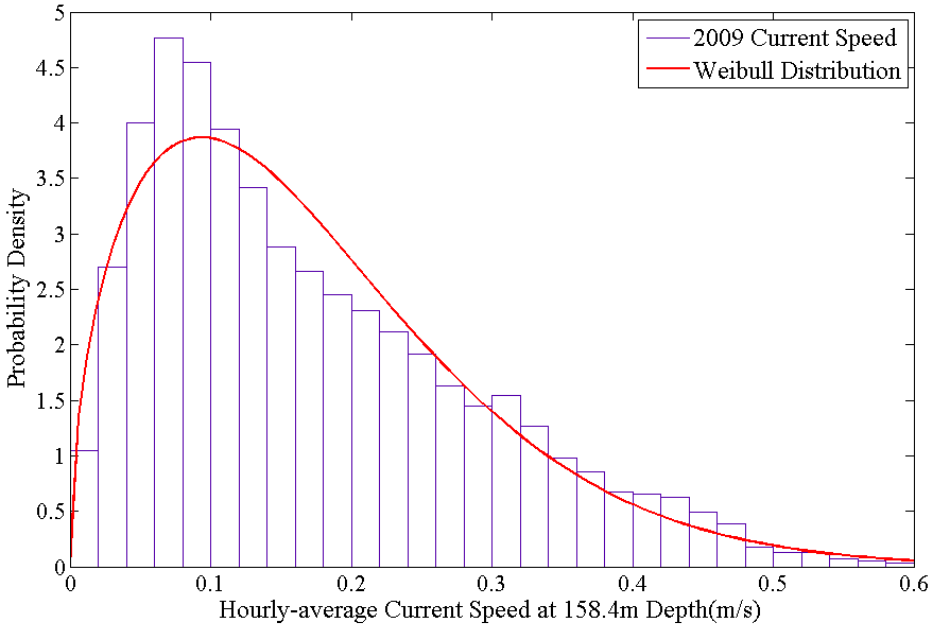

Fig. 26 Current speed distribution and Weibull fitting at 158m for 2009

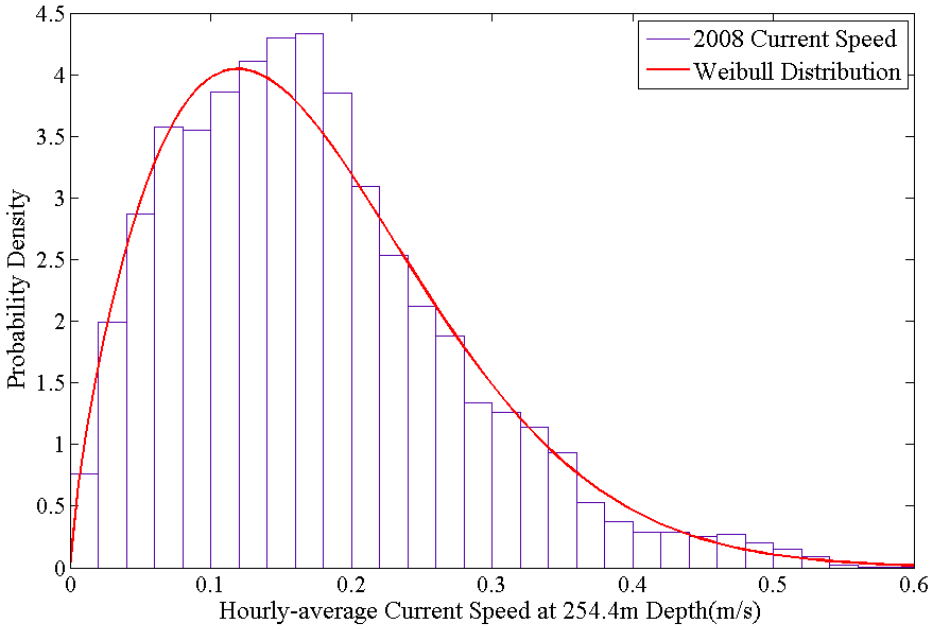

Fig. 27 Current speed distribution and Weibull fitting at 254m for 2008

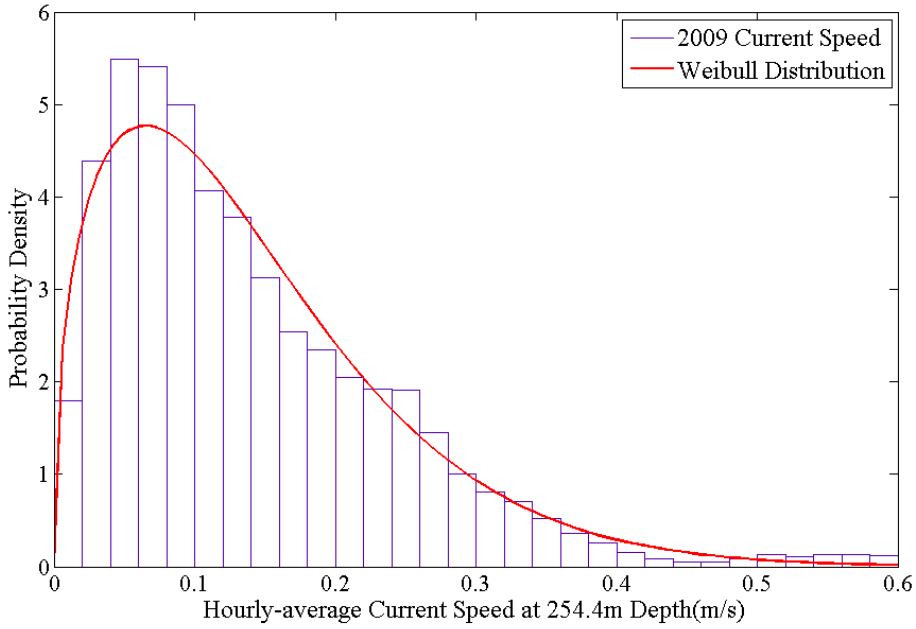

Fig. 28 Current speed distribution and Weibull fitting at 254m for 2009

As shown in Table 6, mean current speed and scale parameter a in 2008 are slightly larger than these in 2009. This can be partially due to the loop-current occurred more often in 2008 at the location of NDBC Station 42886. Except for this, the Weibull distribution equations for 2008 and 2009 are very similar in all depths.

Table 6

Detailed statistical results of current speed in different depths for 2008 and 2009

	Mean (m/s)	a(Scale Parameter)	b(Shape Parameter)	Weibull Distribution Density Fuction
2008 at 62.4m Depth	0.277	0.309	1.607	$Y = 10.61X\text{^}0.61exp[-(X/0.31)\text{^}1.61]$
2009 at 62.4m Depth	0.247	0.274	1.545	$Y = 11.42X\text{^}0.55exp[-(X/0.27)\text{^}1.55]$
2008 at 158.4m Depth	0.198	0.221	1.586	$Y = 17.38X\text{^}0.59exp[-(X/0.22)\text{^}1.59]$
2009 at 158.4m Depth	0.174	0.193	1.506	$Y = 17.94X\text{^}0.51exp[-(X/0.19)\text{^}1.51]$
2008 at 254.4m Depth	0.174	0.195	1.648	$Y = 24.38X\text{^}0.65exp[-(X/0.20)\text{^}1.65]$
2009 at 254.4m Depth	0.141	0.154	1.516	$Y = 25.85X\text{^}0.52exp[-(X/0.15)\text{^}1.52]$

3.4 Wave Joint Probability

It is common in design practice to generate sea surface realizations using a modified two parameter JONSWAP wave elevation spectrum. These two key parameters in JONSWAP model are the significant wave height, Hs, and the peak period, Tp.

Therefore these two parameters were chosen to generate the Joint probability contour in this study. After the data checking and processing, 20516 sets of significant wave height and peak period data during the 35 months were chosen for the derivation of the joint probability contour. Each set contains the hourly averaged significant wave height and peak period at a given hour.

MATLAB is employed to generate the joint probability density matrix of significant wave height (Hs) and peak period (Tp). In order to make the contour curves more smoothly shaped and demonstrate the major trend, we delete some of the outliers to make the contour plot function work smoothly. The result is a 24×24 matrix. The numbers in each row and column indicates the numbers of data within a certain range. For example, the figures in column 1 are numbers of peak periods within the range of significant wave height from 0 to 0.5m. In the same way that the values in row 1 are numbers of significant wave heights within the range of peak period from 19 to 20 second. From Table 3 we can infer the shape for Hs-Tp joint probability contour by institution. The majority of peak period in second column where the significant wave heights are between 0.5m and 1m are located within the 5 to 6 second range as shown in Table 7. We can also infer from the matrix that the overall occupancy of data points with significant wave height greater than 3.5m (approximate) is less than 1%. In order to find the analytic distribution of Hs-Tp joint probability, the distribution for individual Hs and

Tp should be found at the first place. In this study, this procedure was performed following the method used by Winterstein et al. (1993) based on the First Order Reliability Method (FORM).

The name of First Order Reliability Method comes from the fact that the performance function $G(\mathbf{X})$ is approximated by the first order Taylor expansion (linearization). The performance function $G(\mathbf{X})$ is used to determine the structures failure probability. When $G(\mathbf{X}) \geq 0$, the structure is safe. If it is assumed that performance function depends on two variables $\mathbf{X}=\{H_s, T_p\}$, the probability of structure failure can be computed by integrating the joint probability density function (PDF) of significant wave height and peak period within the $G(\mathbf{X}) < 0$ region. Both the integrant (Joint PDF of Hs and Tp) and the boundary of integral ($G(\mathbf{X}) = 0$) should be simplified. In this study, only the simplification of integrant, namely, the Hs-Tp joint probability is taken into consideration.

Table 7

The statistical results for significant wave height and peak period joint probability. The unit for Hs is meter and the unit for Tp is second.

Hs Tp	0-0.5	0.5-1	1-1.5	1.5-2	2-2.5	2.5-3	3-3.5	3.5-4	4-4.5	4.5-5	5-5.5	5.5-6	6-6.5	6.5-7	7-7.5	7.5-8	8-8.5	8.5-9	9-9.5	9.5-10	SUM
19-20	0	0	0	0	0	0	0	0	0	0	0	0	0	0	0	0	0	0	0	0	0
18-19	1	0	0	0	0	0	0	0	0	0	0	0	0	0	0	0	0	0	0	0	1
17-18	4	0	0	0	0	0	0	0	0	0	0	0	0	0	0	0	1	0	0	0	5
16-17	3	0	0	0	0	0	0	0	0	0	1	0	0	0	0	0	1	0	0	0	5
15-16	2	1	0	0	0	1	1	0	0	0	1	2	3	1	1	0	0	1	0	1	15
14-15	2	0	0	3	2	0	0	0	0	3	1	3	3	0	1	2	0	0	0	1	21
13-14	2	0	0	1	0	2	1	0	0	1	0	1	2	0	0	0	1	3	1	0	15
12-13	2	0	0	1	0	1	0	1	2	2	3	2	0	0	1	1	1	0	0	1	18
11-12	5	2	0	3	0	2	1	9	4	3	1	2	3	1	0	0	2	0	0	0	38
10-11	10	3	1	9	10	25	13	23	6	1	2	0	1	2	0	0	0	0	0	0	106
9-10	57	37	13	62	117	71	85	34	29	14	0	0	0	0	0	0	0	0	0	0	519
8-9	180	159	260	480	341	233	107	56	18	1	0	0	0	0	0	0	0	0	0	0	1835
7-8	510	1022	1384	983	493	238	40	11	0	0	0	0	0	0	0	0	0	0	0	0	4681
6-7	961	2028	1568	459	105	14	0	0	0	0	0	0	0	0	0	0	0	0	0	0	5135
5-6	1123	2239	756	50	0	0	0	0	0	0	0	0	0	0	0	0	0	0	0	0	4168
4-5	1441	1951	182	0	0	0	0	0	0	0	0	0	0	0	0	0	0	0	0	0	3574
3-4	276	103	0	0	0	0	0	0	0	0	0	0	0	0	0	0	0	0	0	0	379
2-3	1	0	0	0	0	0	0	0	0	0	0	0	0	0	0	0	0	0	0	0	1
SUM	4580	7545	4164	2051	1068	587	248	134	59	25	9	10	12	4	3	3	5	5	1	3	20516

Winterstein et al. (1993) fit the field data on significant wave height to obtain a specific three-parameter (h_0 , r and h_1) truncated Weibull cumulative distribution function (CDF). The Weibull CDF for $h>h_1$ can be expressed approximately as a standardized normal distribution,

$$F_{H_s}(h) = 1 - exp\left[-(h/h_0)^r + (h_1/h_0)^r \right] \cong \Phi(U_1) \qquad (7)$$

where h_0 is equivalent to the scale parameter a of Weibull probability distribution function, h_1, the arbitrary cutoff significant wave height, r, equivalent to the gust parameter b of Weibull probability distribution function. $\Phi(.)$ is the standard cumulative normal distribution function, and U_1, the first standard normal variable for randomly selected significant wave height. The significant wave heights below 0.2m and their associated peak periods were not included in the calculation of F_H because the cutoff significant wave height is set at 0.2m. Following the maximum log-likelihood method described in the Chapter 2, the two parameters a and b of Weibull probability distribution function are estimated as shown in Eqn.(8).

$$f(h|a,b) = 1.1802 x^{0.466} exp\left[-(h/1.160)^{1.466} \right] \qquad (8)$$

where a is 1.160 (scale parameter) and b is 1.466 (gust parameter). Thus, r and h_0 in Eqn.(7) are determined. The truncated Weibull CFD of Eqn.(7) can be approximately obtained by integrating Eqn.(8) from h_1 to positive infinity where h_1=0.2m as the cutoff significant wave height. Eqn.(9) is the fitted Weibull CDF of the EPRMS data

which can be employed to generate the standard normal distribution variable U_1. Therefore the mapping of random variable Hs and U_1 is obtained.

$$F_{H_s}(h) = 1 - exp\left[-(h/1.160)^{1.466} + (0.2/1.160)^{1.466}\right] \quad (9)$$

In the analysis by Winterstein et al. (1993), the peak period is assumed conditional normal distribution with its mean satisfying the equation

$$\mu_{T_p} = mH_s^n, \quad (10)$$

where μ_{T_p} is the conditional mean of peak period when Hs is given, and *m* and *n* are fitted based on the recorded data, which are given in Eqn.(11). To obtain the regression curve of significant wave height and mean peak period, we divide the peak period data into groups by the value of their corresponding significant wave heights. By sorting the significant wave height from the cutoff value 0.2m to the largest, the peak periods were divided into 21 groups. Each group has 1000 sets of data except for the last group which has 516 sets. Then we use the normal distribution to fit the peak period data and find the mean value of the peak period in each group of given Hs. The standard deviation of peak period for each group has also been calculated to derive the COV in Eqn.(12). COV is defined as the coefficient of variation defined as the ratio of its standard deviation to its mean. Finally we use least square method to fit the exponential regression curve for mean value of Tp as shown below. And the equation of the regression line is,

$$E\left[Tp/Hs\right]=6.35Hs^{0.309} \tag{11}$$

Eqn.(12) is used to map T_p into U_2, which is a standard normal variable,

$$T_{P/Hs}=6.35Hs^{0.309}\left(1+\mathrm{COV}\times U_2\right) \tag{12}$$

where U_2 is the second standard normal variable for the peak period. COV is calculated and equal to 0.15 in this study. The expression of U_2 shown in Eqn.(13) indicates that U_2 obey the standard normal distribution,

$$U_2=\left(T_p-\mu_{T_p/H_s}\right)/\sigma_{T_p/H_s} \tag{13}$$

where μ_{T_p/H_s} is the conditional mean of peak period as shown in Eqn.(10) and σ_{T_p/H_s} is the standard deviation for peak period at given significant wave height. We can thus relate *Tp* to the second standard normal variable. Meanwhile based on the existed relation between a given *Hs* and the mean *of Tp,* the relation between *Tp* and U_1, U_2 can be easily found. The environmental contour consists of all the possible $\{Hs,Tp\}$ combinations with the equidistance from the origin, forming a circle with radius β' with the center at the origin of the standard normal plane.

$$U_2=\sqrt{\beta'^2-U_1^2} \tag{14}$$

For extreme wave condition, the probability of occurrence of a storm with return period *Tr*, conditional on an event is given as

$$P_{\mathrm{occ,event}}=1/\nu T_R=1-\Phi\left(\beta'\right) \tag{15}$$

Hurricanes at a given location in the Gulf of Mexico were assumed to occur independently with an annual rate of occurrence, ν, say 0.1, per year (Winterstein et al., 1995). Therefore the U_2 can be solved by the Eqn.(14). For example, if we intended to plot the 100-year storm contour, $P_{\text{occ,event}} = 1/\nu T_R$ =1/0.1*100=0.1 and β' =1.2816 which is the resulting radius used to generate the 100-year contour in U-space. For any given U_1, the corresponding U_2 could be solved by Eqn.(14) and Eqn.(15). The 'cap', namely the largest significant wave height with its corresponding peak period in each contour should lie on the regression line shown in Eqn.(11) illustrated while $U_1 = \beta'$ and U_2 is equal to zero. Obviously, Eqn.(14) cannot be used in our case to predict storm contours based on the statistics of general wave condition (not storm condition). The available data for only 35-month duration are too short to predict the significant wave height and peak period with large return period, such as for 100-year or 1000-year storm. Because the overall data sets with significant wave heights larger than the cutoff threshold Winterstein set for 'storm' are no more than 50 counts. However, Eqn.(14) is still applicable to determine the joint probability contour for yearly cases. Detailed transformation process and supplemental figures were attached in Appendix C.

The joint probability density contour and the regression line are plotted in Fig.29. In any cross section of a given x (Hs) value the peak period generally represent the normal distribution and the data of significant wave height represents Weibull distribution of a

given y (Tp) value. The data along the regression line are of the highest frequency of occurrence with the peak period taking the value of the conditional mean. We choose 75%, 90%, 95%, 99% and 99.9% five contours to draw the Fig.29. If we call the position with largest probability density as 'origin' in x-y plane, the percentage for each contour indicates the proportion of data on the side of the origin of standard normal plane when the plane is divided into two parts by a tangent line drawn at any point of defined contour. We also drew the joint probability contour for the cutoff significant wave height h_1=0. However, the plot is similar to Fig.29, and for brevity, it is not shown here.

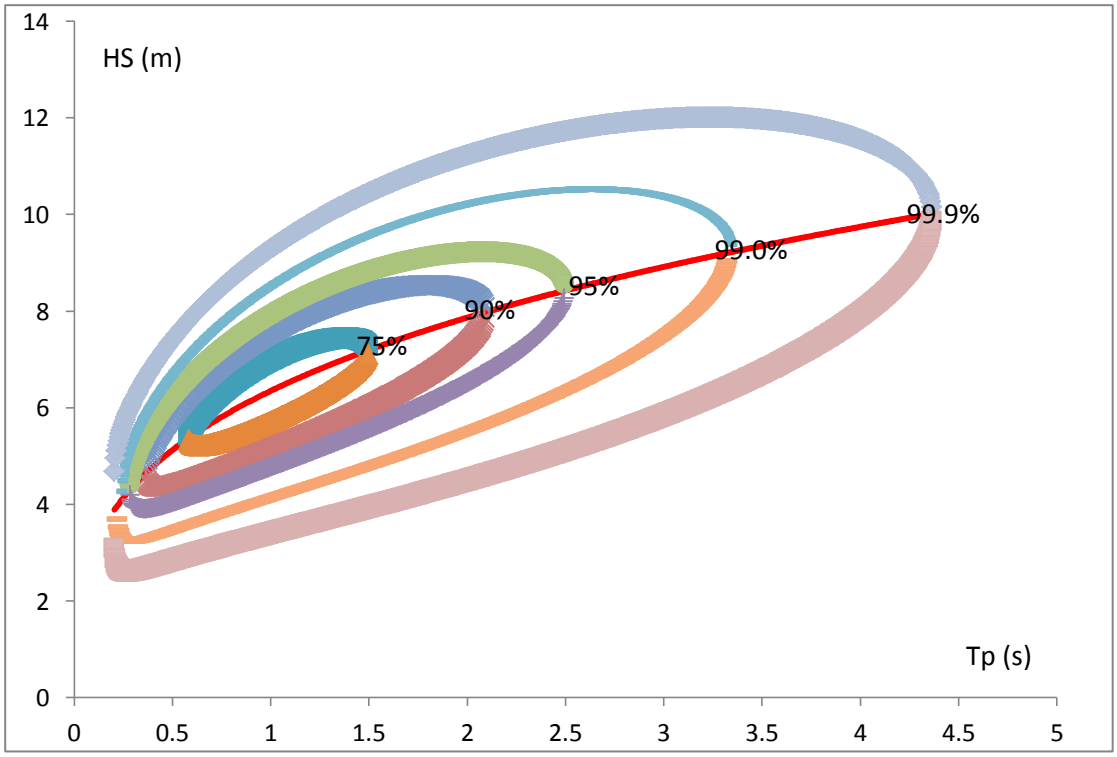

Fig. 29 The joint probability density contour of three years wind data and the regression line

Compared with the environmental contour for extreme weather condition derived by Winterstein et al. (1993), the two regression lines are similar to each other as shown in the Fig.30. Since Winterstein et al. (1993) derived the truncated Weibull distribution for extreme weather condition with 20-year data, the scale parameter and gust parameter in Weibull distribution are much greater than that we have derived based on the 3 year field data (Winterstein a=6.25,b=2.29; Constitution a=1.17,b=1.48). However, both joint probability contours basically have the identical shape. It is also noticed that due to the difference in Coefficient of Variance (COV) in conditional normal distribution of peak period (Winterstein COV=0.06, Constitution Spar COV=0.15), the contour generated by Constitution data has a clearly trend of "inflating" while the Winterstein's contour is relatively 'compact' as shown in Fig.31.

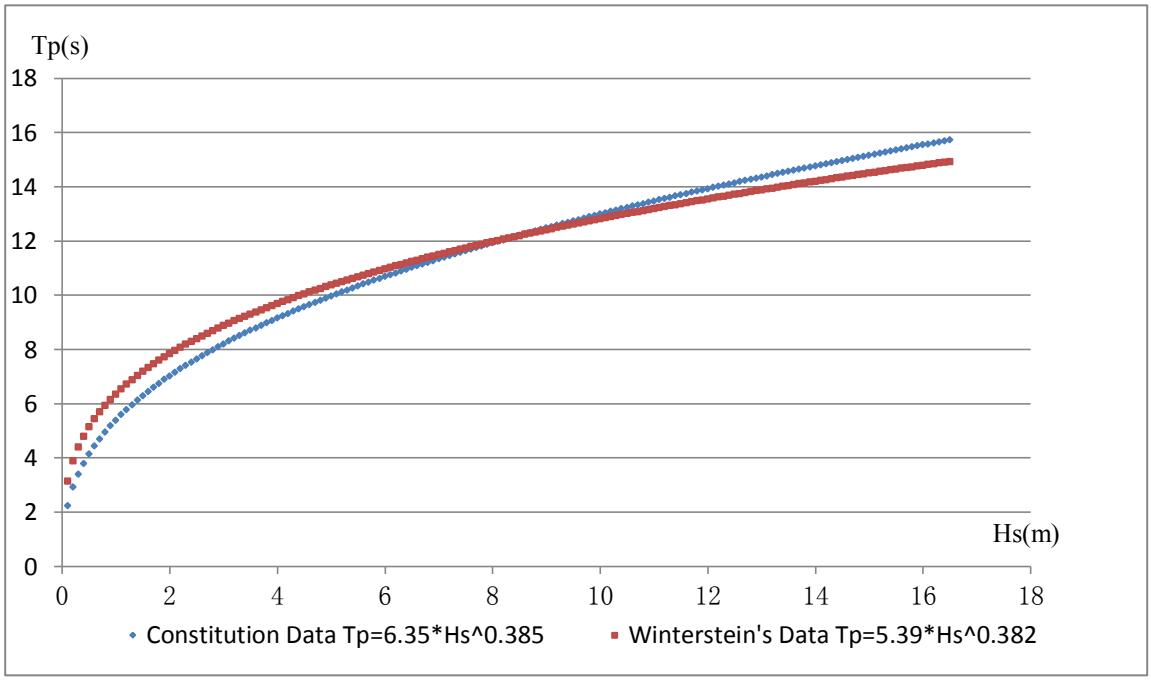

Fig. 30 Hs-Tp regression lines for Constitution data and Winterstein's data

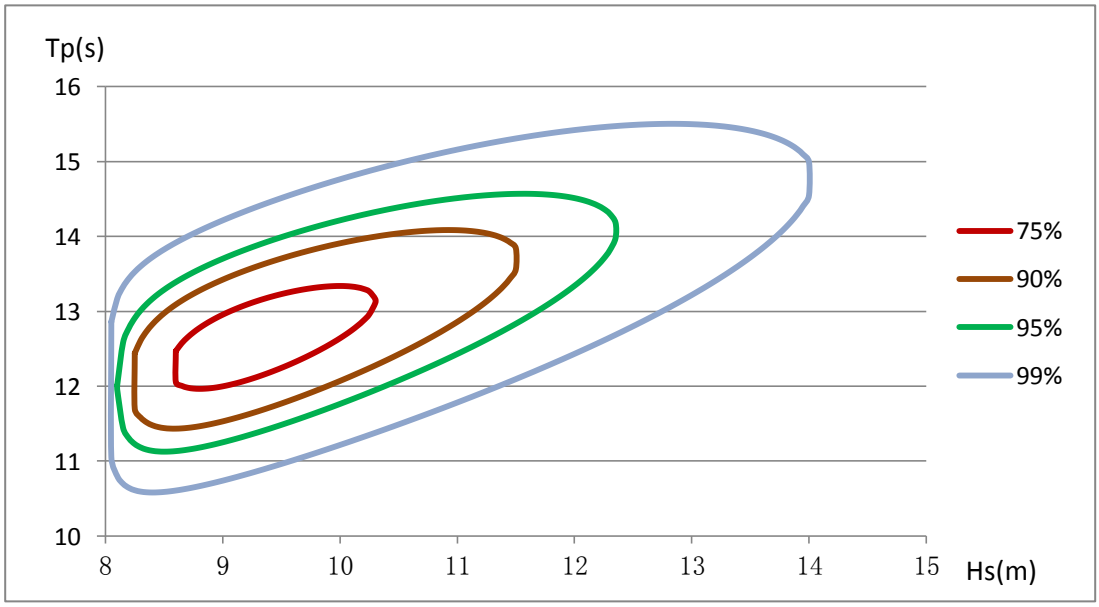

Fig. 31 Hs-Tp Contour for Extreme Weather Condition in Gulf of Mexico Derived by Winterstein

4. CONCLUSION

Based on the EPRMS data recorded from June 2007 to April 2010 at the site of Constitution and current data recorded at NDBC Station 42886, which was almost 10 kilometer southeast from Constitution, we derived the statistics and probability distribution of wind speed, current velocity, and joint probability distribution of the significant wave height and peak period. The directions and speeds of winds in different seasons are visualized using rose diagram. In summary, the following main results have been obtained.

1. The wind speed distribution is fitted using a two-parameter Weibull distribution. The comparison among the Weibull distribution for each of three years shows good agreement in both scale parameter and gust parameter, which indicates consistency in average wind speed and the wind gustiness. Winds most blow from the East to West. However, winds of large speed caused by hurricanes or storms usually blow from the Southeast to Northwest or from Northwest to Southeast.
2. The large current speed occurred during long period such as one month or two months always due to the loop-current. Large wind can affect the surface current speed but with a limited depth.
3. Because the recorded data available to us is limited for only 35 month, the joint

probability (Hs & Tp) contour obtained in this study should not be used to address the probability of extreme waves accurately. In the 35-month period, the hourly-average significant wave heights larger than 3.5 meters were less than 250 counts. Significant wave heights larger than 8 meters were less than 50 and 8 m is the cutoff significant wave height used by Winterstein et. al. (1993) for extreme wave condition. Nevertheless, the relationship between the mean of the peak period and associated significant wave height is very similar to the result derived by Winterstein et al. (1993) based on 20-year data. The joint probability distribution derived in this study can be used in the yearly simulation of offshore structures for the studies of their fatigue life.

REFERENCES

Dyrbye, C., Hansen, S.O., 1997. Wind Loads on Structures, Wiley, New York.

Irani, M.B., Perryman, S.R., Geyer, J.F., Von Aschwege, J.T., 2007. Marine monitoring of Gulf of Mexico deepwater floating systems. Proceedings of Offshore Technology Conference 18626.

Jaramillo, O.A., Borja, M.A., 2004. Wind speed analysis in La Ventosa, Mexico: a bimodal probability distribution case. Renewable Energy 29, 1613-1630.

Jowder, F.A.L., 2006. Weibull and Rayleigh distribution functions of wind speed in Kingdom of Bahrain. Wind Engineering 30 (5), 439-446.

Monahan, A.H., 2006. The probability distribution of sea surface wind speeds part I: theory and sea winds observations. Journal of Climate 19, 497-520.

Prislin, I., Rainford, R., Perryman, S., Shilling, R., 2005. Use of field monitored data for improvement of existing and future offshore facilities. SNAME Maritime Technology Conference & Expo and Ship Production Symposium 113, 437-441.

Rehman, S., Halawani, T.O., Husain, T., 1994. Weibull parameters for wind speed distribution in Saudi Arabia. Solar Energy 53 (6), 473-479.

Seguro, J.V., Lambert, T.W., 2000. Modern estimation of the parameters of the Weibull wind speed distribution for wind energy analysis. Journal of Wind Engineering and

Industrial Aerodynamics 85, 75-84.

Winterstein, S.R., Ude, T.C., Cornell, C.A., Bjerager, P., Haver, S., 1993. Environmental parameters for extreme response: inverse FORM with omission factors. Proceedings of the ICOSSAR-93, Innsbruck, Austria.

Winterstein, S.R., Kumar, S., Kleiven, G., 1995. Environmental contours and extreme response of deep-water floating structures. Proceedings of the 10th Engineering Mechanics Specialty Conference, ASCE 2, 1187-1190.

APPENDICES

Appendix A: Figures of wind speed monthly distribution

Listed below are figures of monthly wind speed distribution from June 2007 to April 2010. We choose two empirical distributions to fit the monthly wind speed, the red curve for Weibull distribution and the blue curve for lognormal distribution. The lognormal distribution usually has a better fitting on the portion with large probability density. However, Weibull distribution has a better fitting for large wind with less probability density, which is also we highly concerned about. And also, for long-term data, such as yearly wind data, we can always see that the Weibull Distribution has better performance than other empirical distributions.

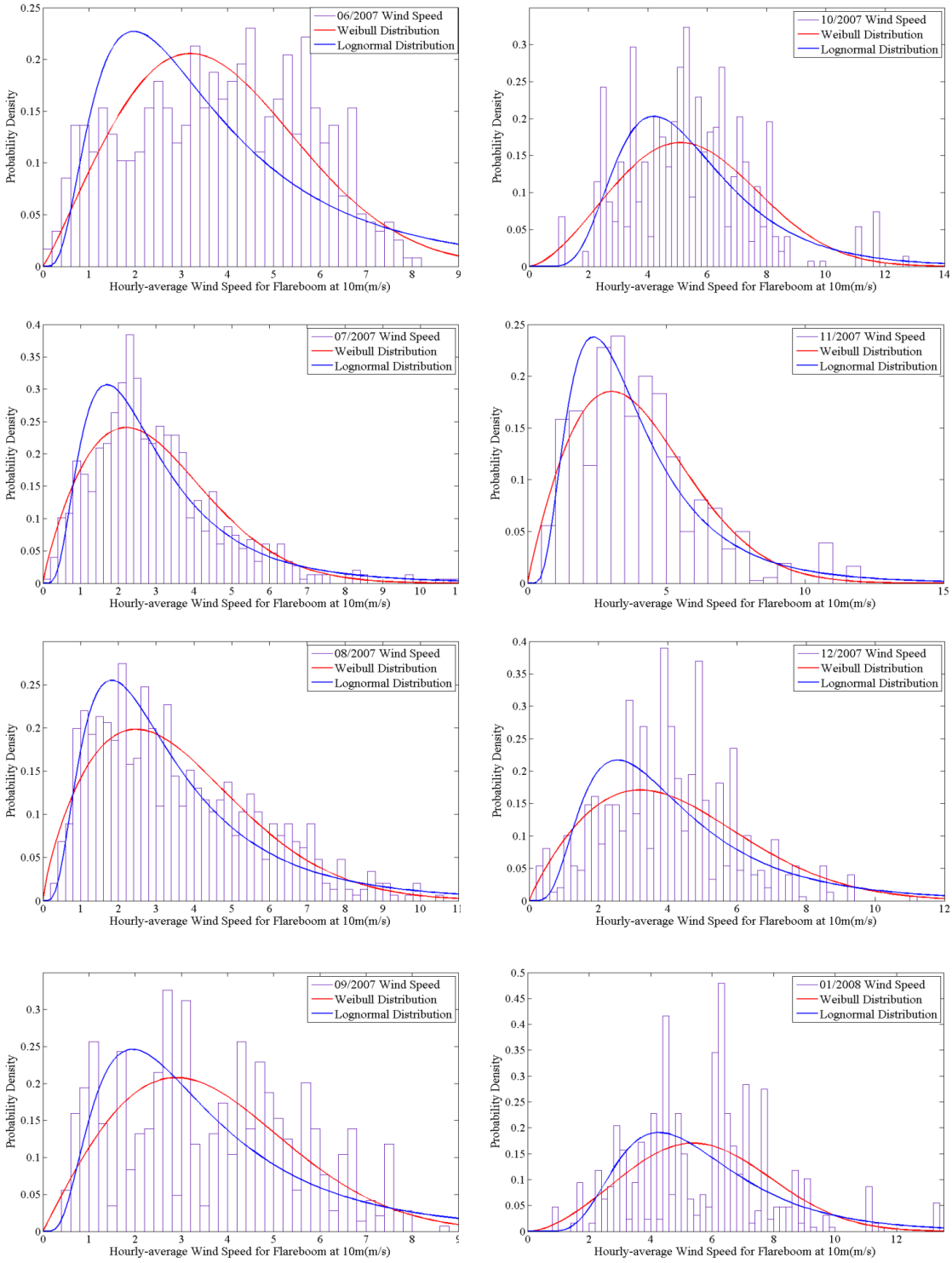

Figure A-1. Monthly wind speed distribution and Weibull and lognormal fitting from Jun. 2007 to Jan. 2008

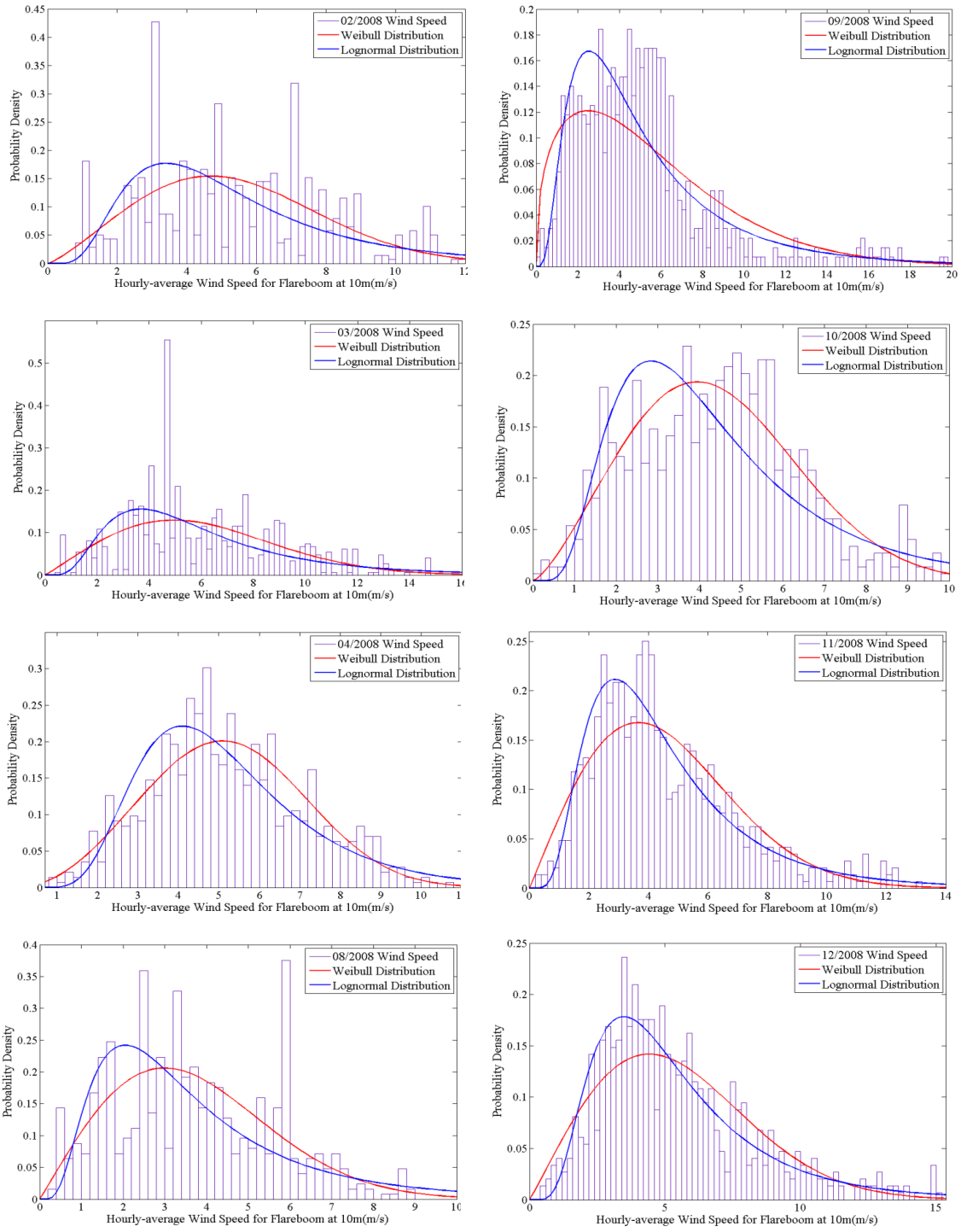

Figure A-2. Monthly wind speed distribution and Weibull and lognormal fitting from Feb. 2008 to Dec. 2008

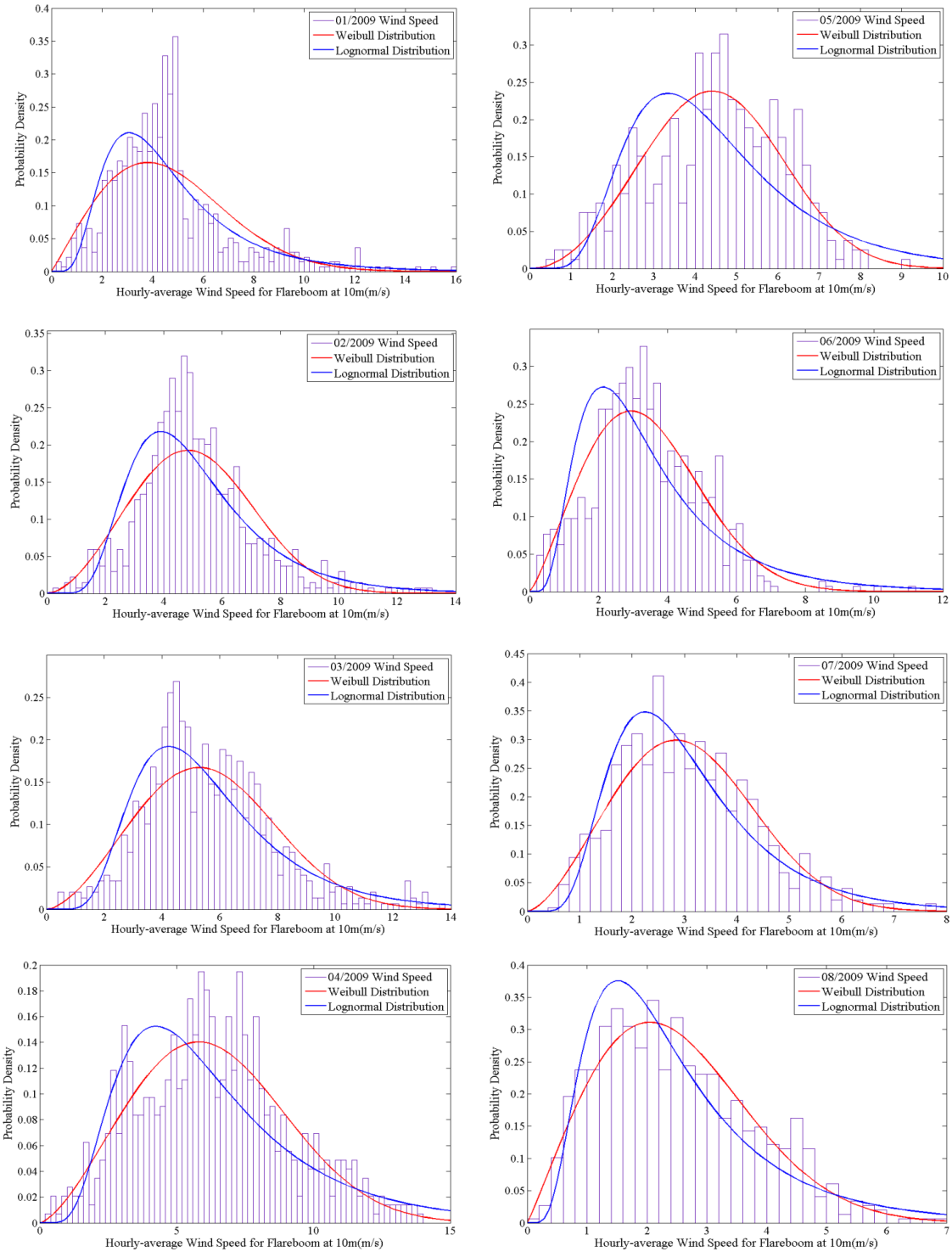

Figure A-3. Monthly wind speed distribution and Weibull and lognormal fitting from Jan. 2009 to Aug. 2009

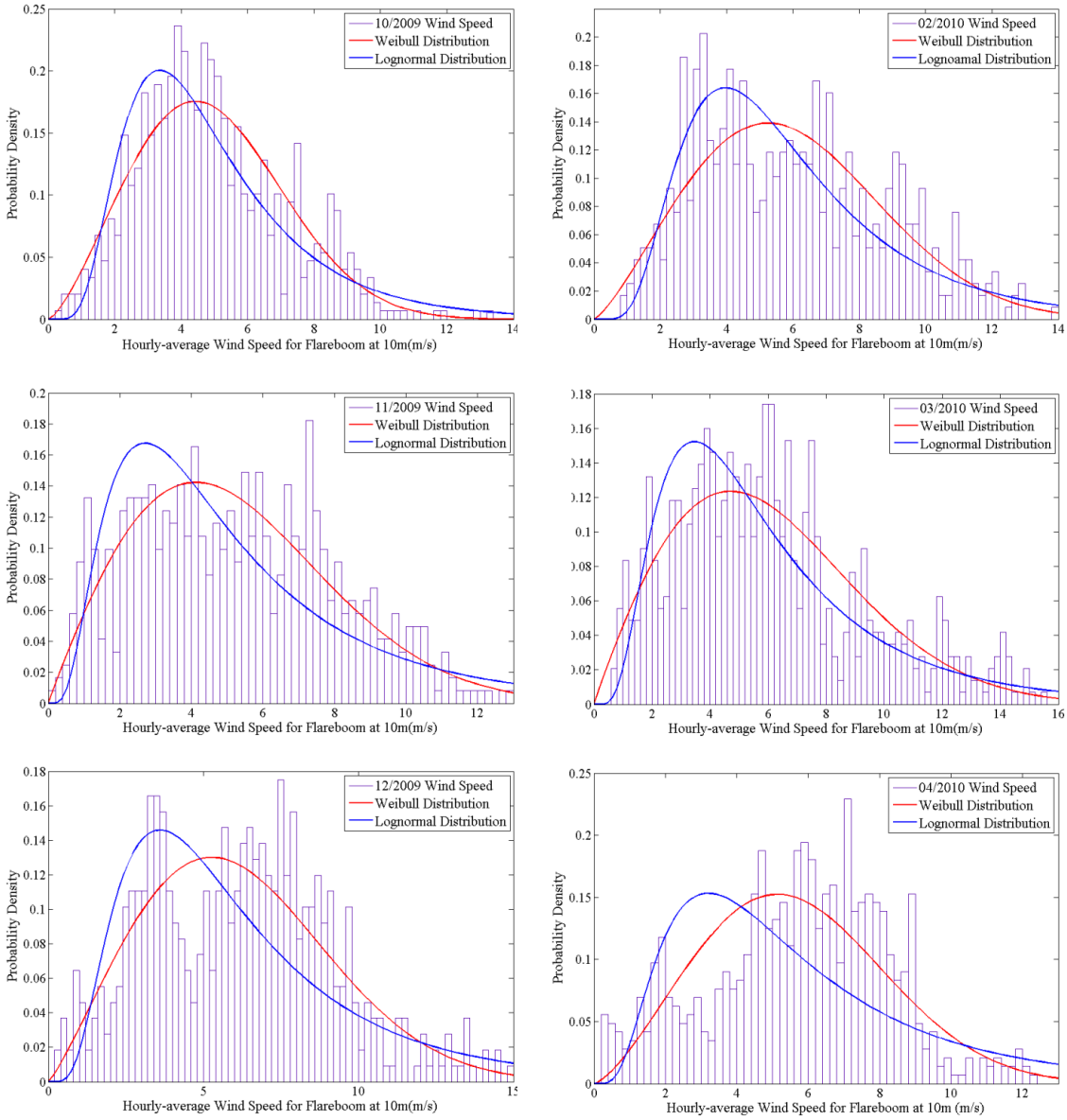

Figure A-4. Monthly wind speed distribution and Weibull and lognormal fitting from Oct. 2009 to Apr. 2010

Appendix B: Figures of current speed monthly distribution for depths 62.4m, 154.4m and 254.4m

Figures of monthly current distributions and fittings at three different depths were given in this appendix. The data is from January 2008 to December 2009. However, the data for Jan 2008 and Sep 2008 are partially missing. For each depth, there are 22 figures. The first 22 figures are for 62.4m depth and the second 22 figures are for 158.4m depth. The Last 22 figures are for 254.4m depth.

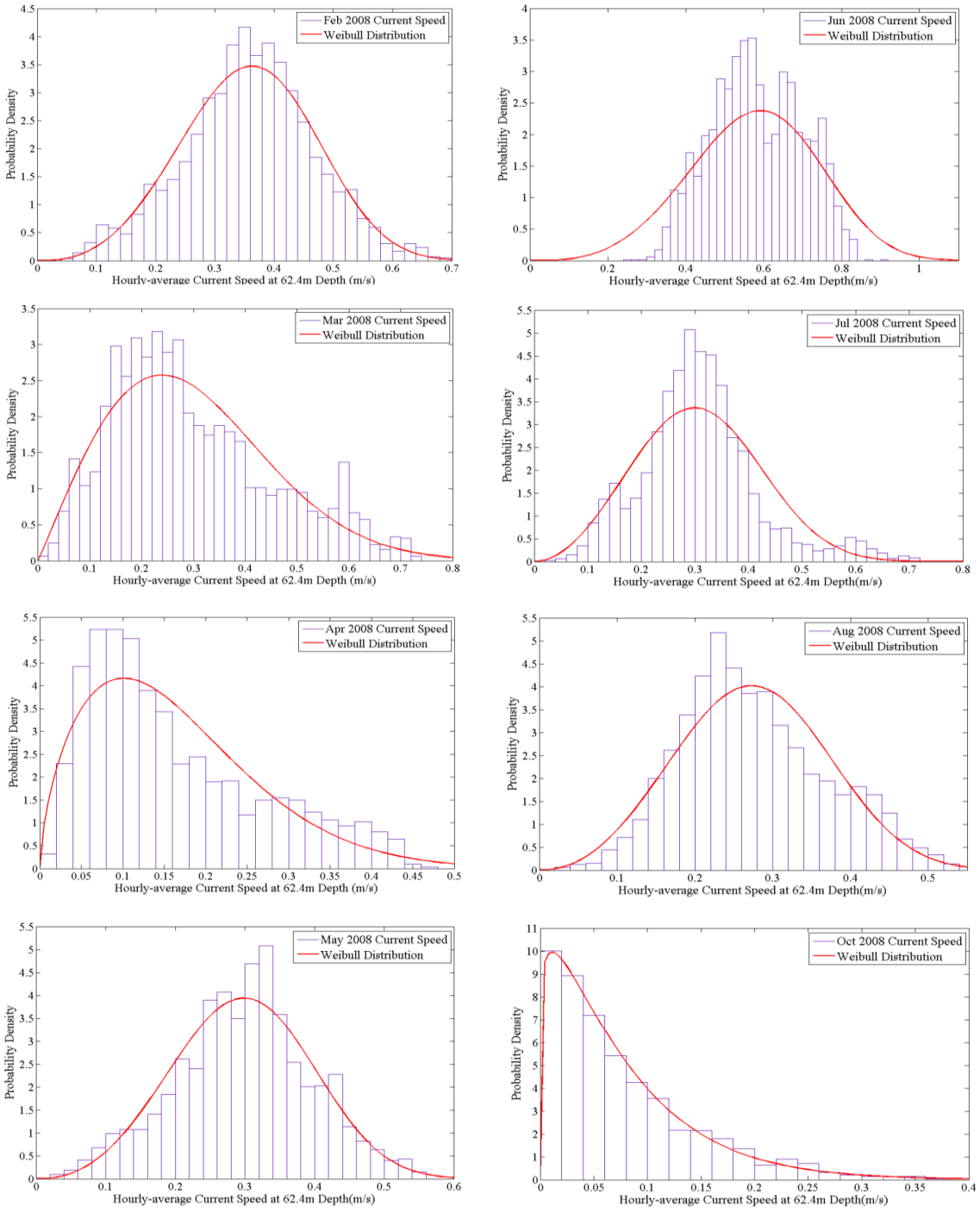

Figure B-1. Monthly current distribution and Weibull fitting from Feb. 2008 to Oct. 2008 at 62.4m depth

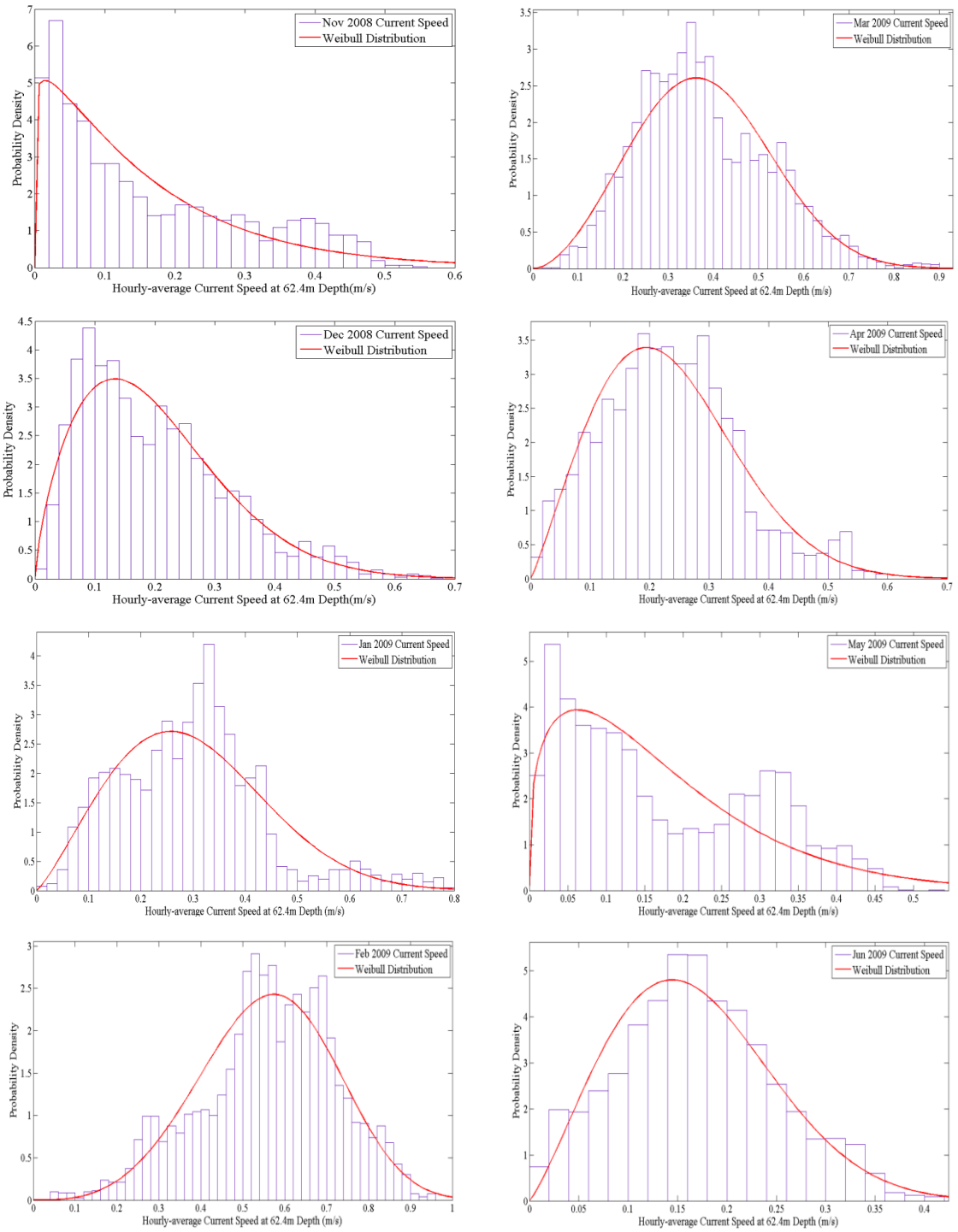

Figure B-2. Monthly current distribution and Weibull fitting from Nov. 2008 to Jun. 2009 at 62.4m depth

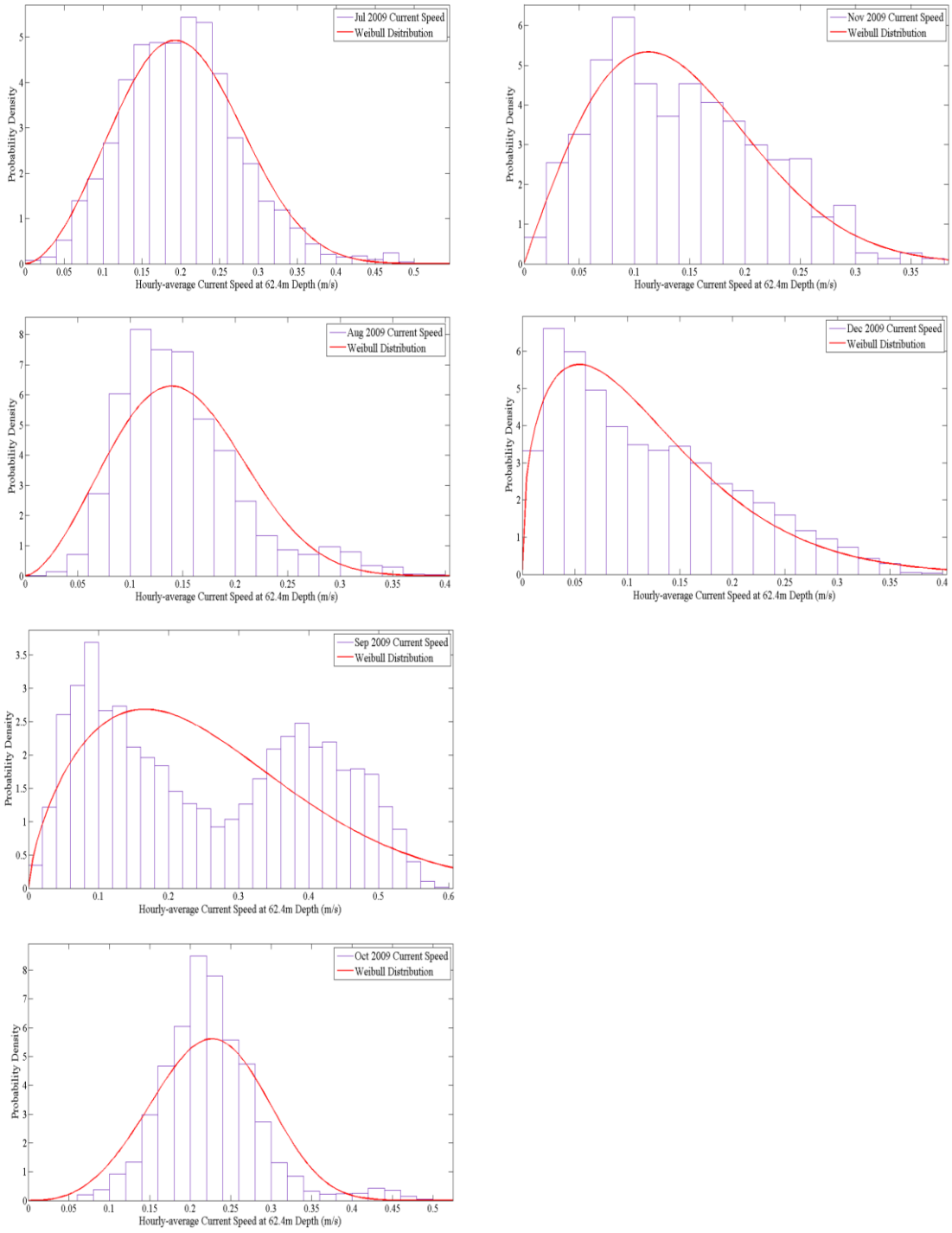

Figure B-3. Monthly current distribution and Weibull fitting from Jul. 2009 to Dec. 2009 at 62.4m depth

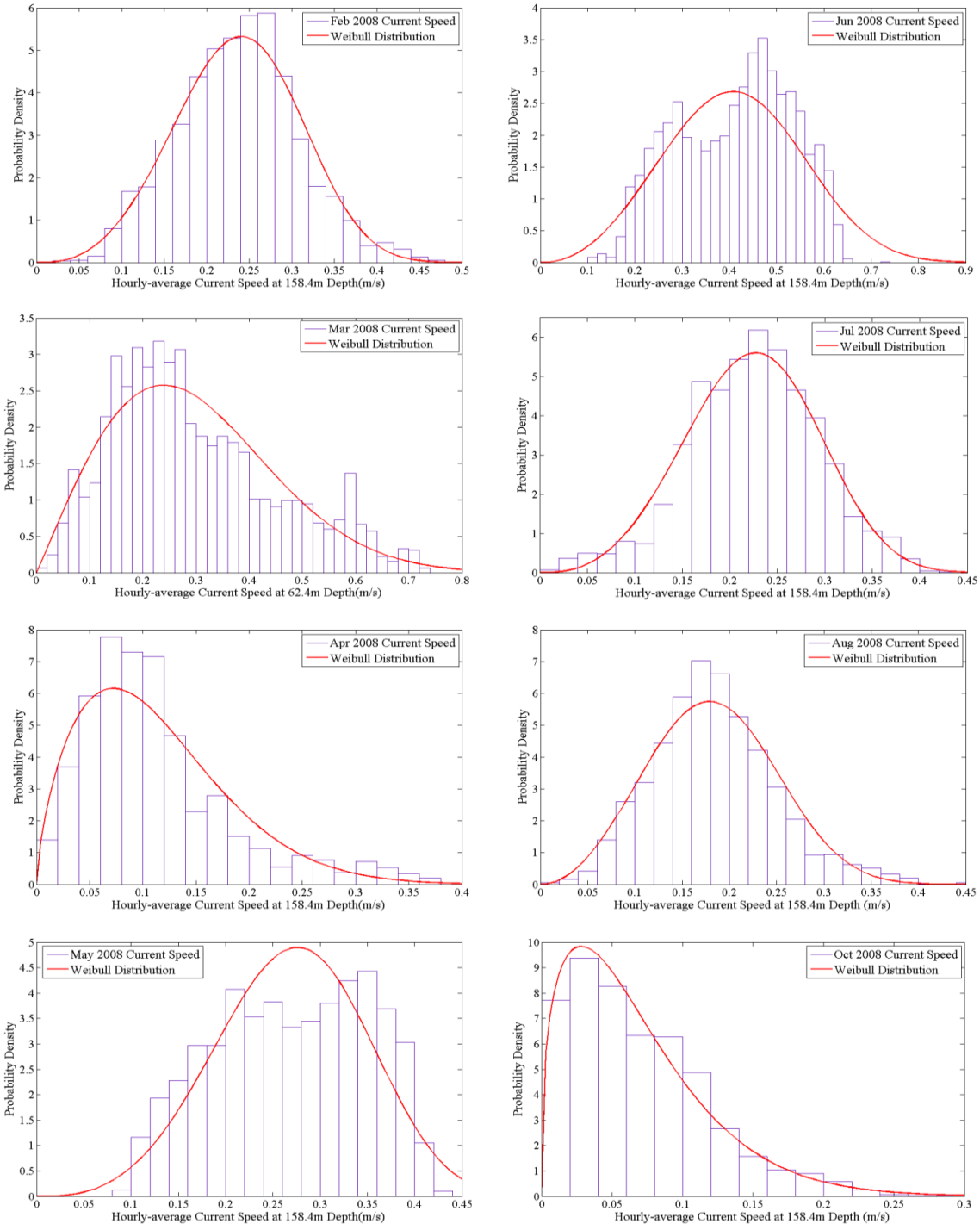

Figure B-4. Monthly current distribution and Weibull fitting from Feb. 2008 to Oct. 2008 at 158.4m depth

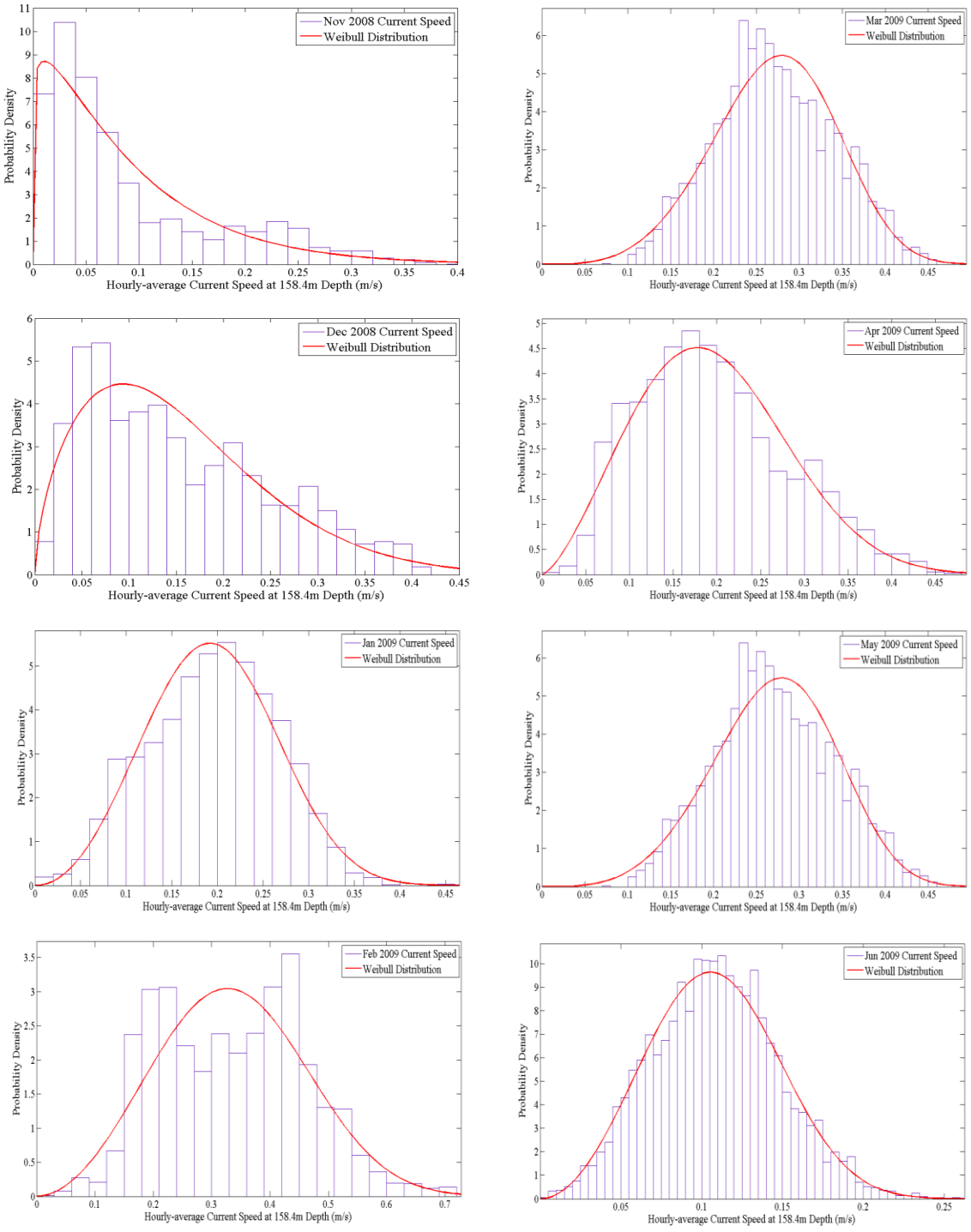

Figure B-5. Monthly current distribution and Weibull fitting from Nov. 2008 to Jun. 2009 at 158.4m depth

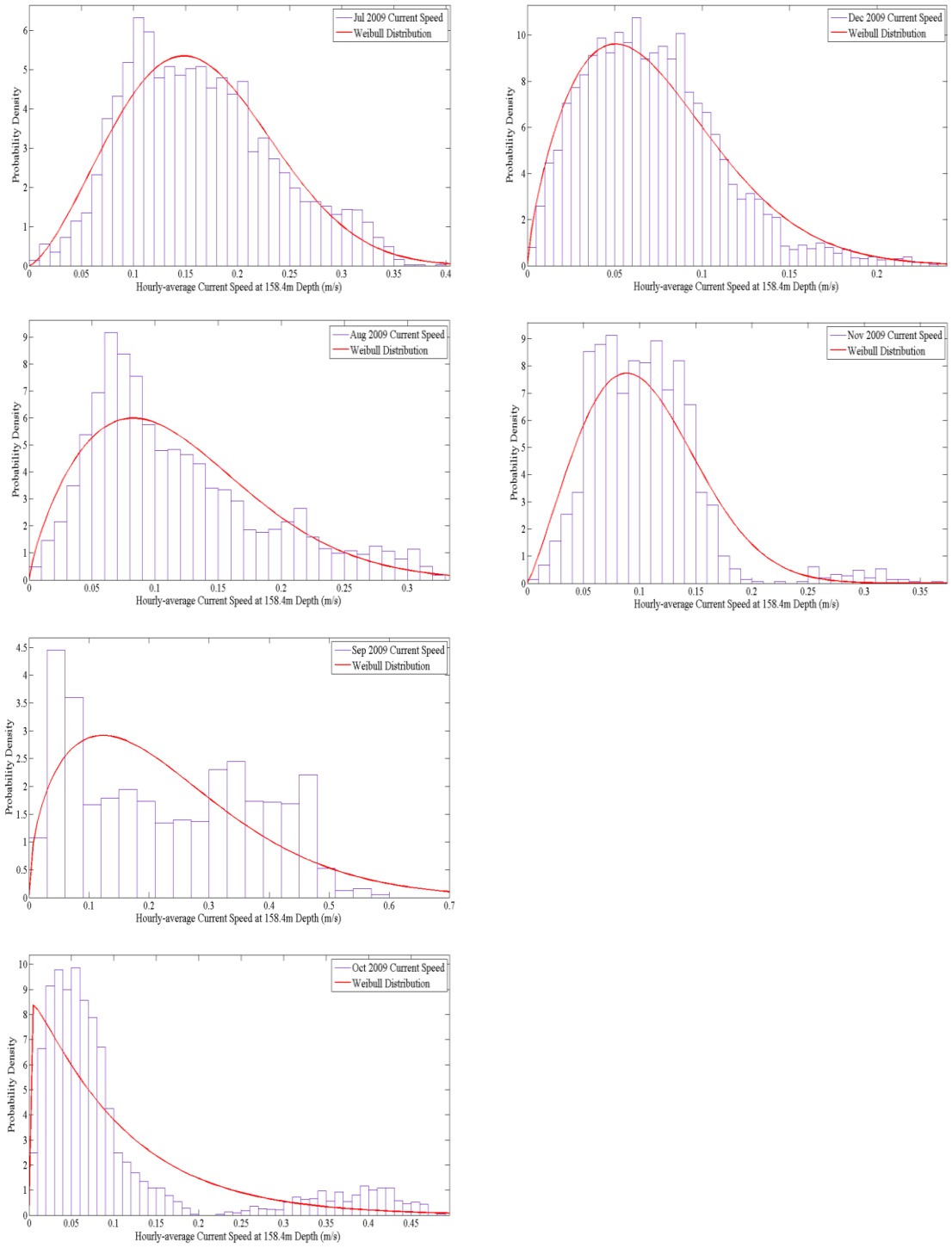

Figure B-6. Monthly current distribution and Weibull fitting from Jul. 2009 to Dec. 2009 at 158.4m depth

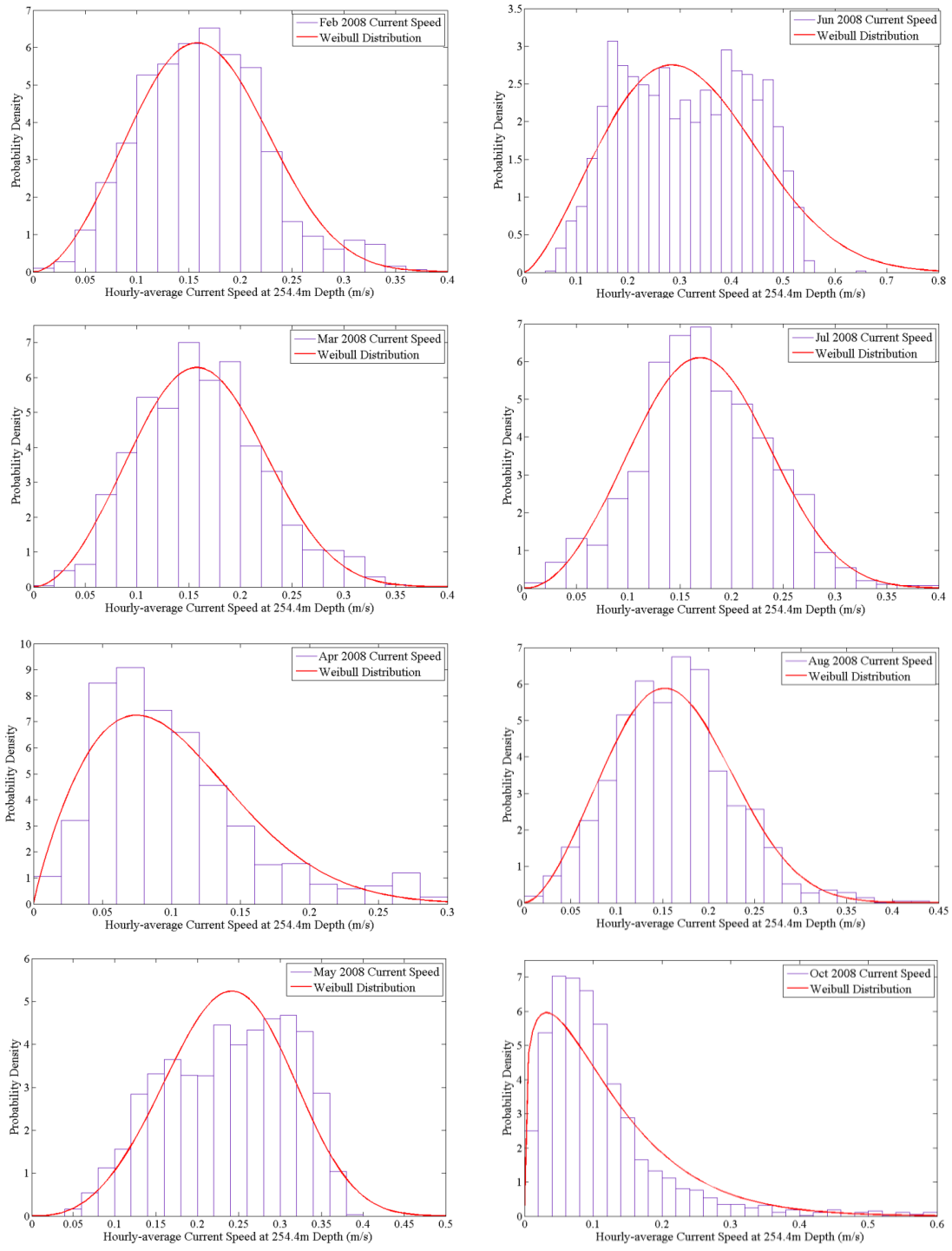

Figure B-7. Monthly current distribution and Weibull fitting from Feb. 2008 to Oct. 2008 at 254.4m depth

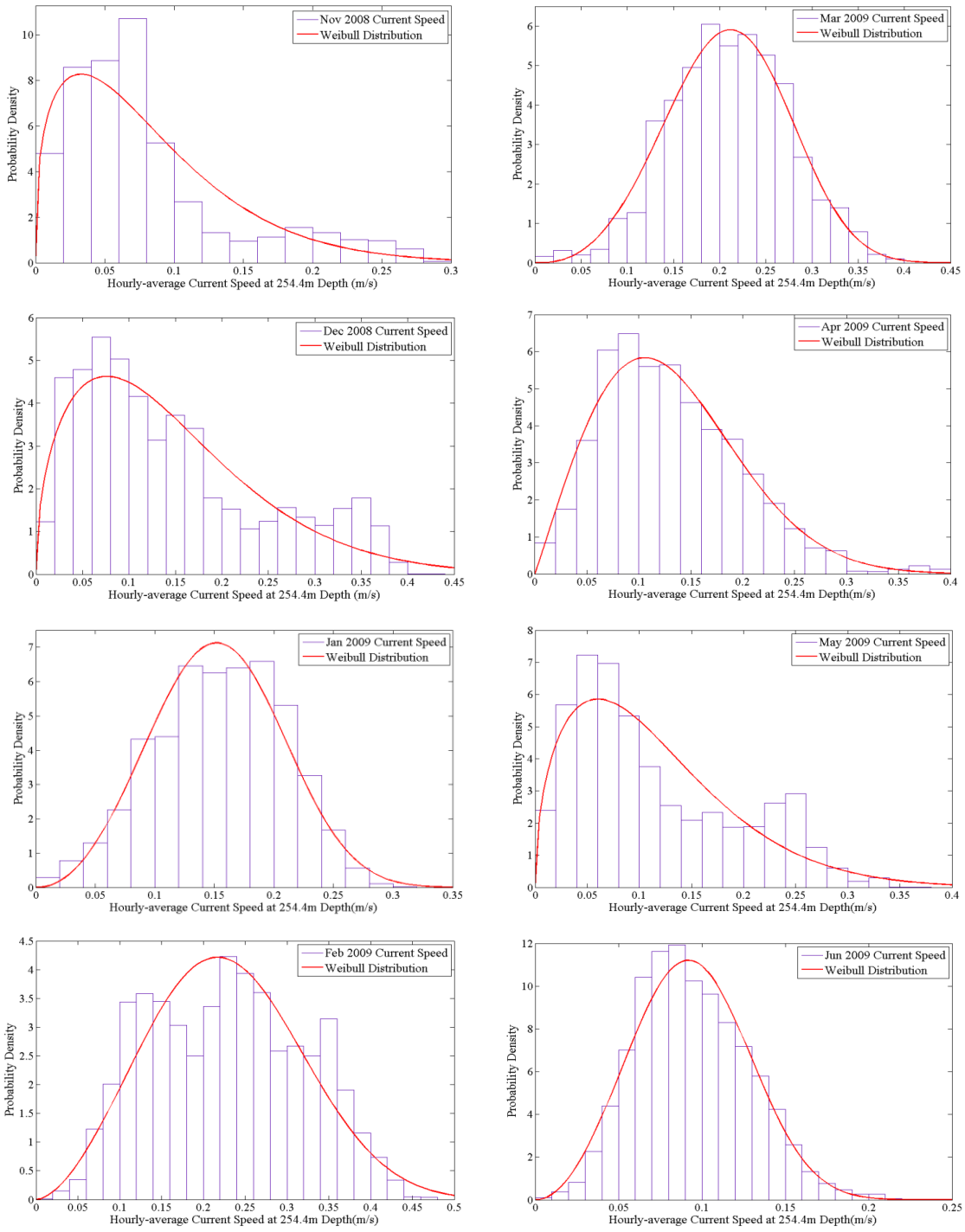

Figure B-8. Monthly current distribution and Weibull fitting from Nov. 2008 to Jun. 2009 at 254.4m depth

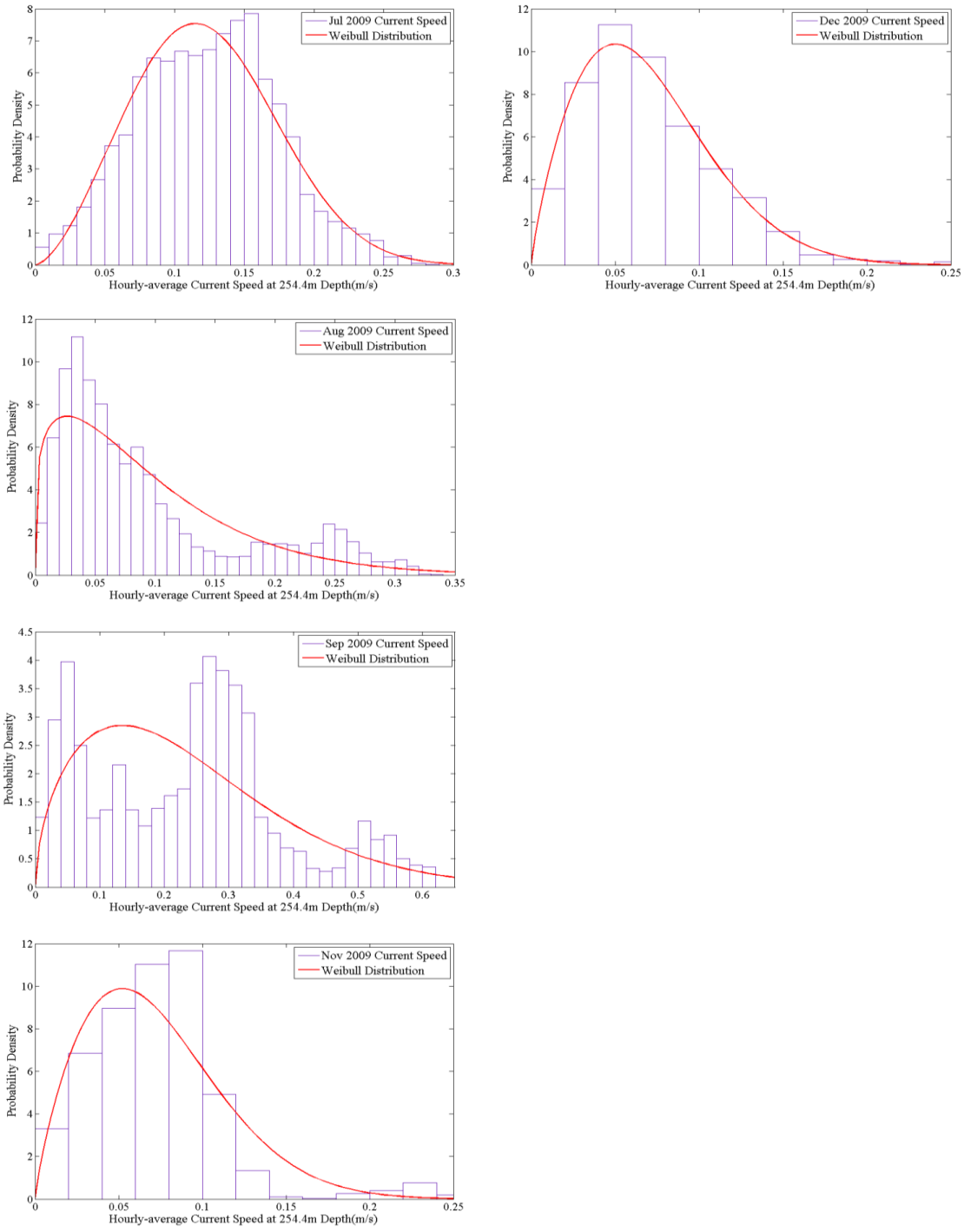

Figure B-9. Monthly current distribution and Weibull fitting from Jul. 2009 to Dec. 2009 at 254.4m depth

Appendix C: Supplemental figures for joint probability contour

The 35 months significant wave height (Hs) has been modeled as two-parameter Weibull distribution.

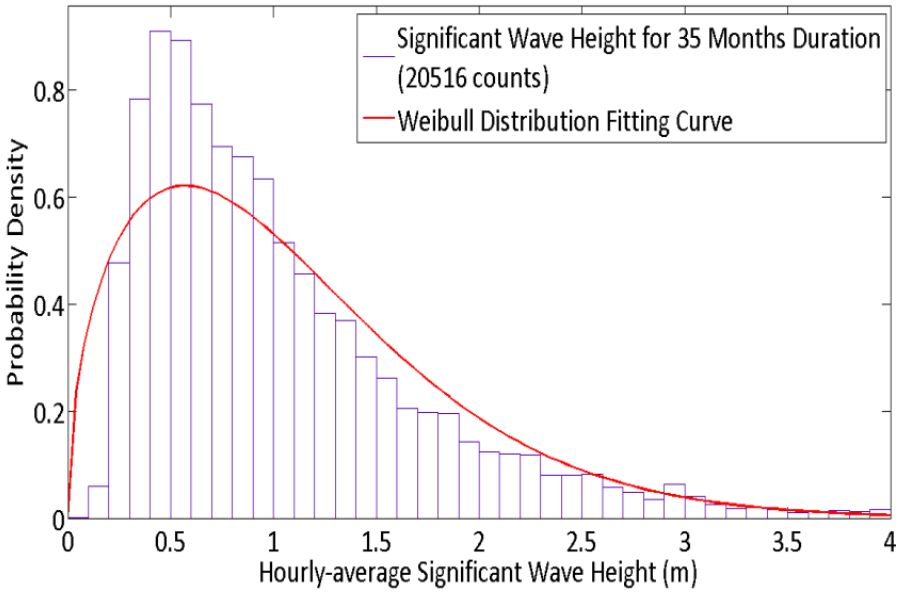

Figure C-1. Weibull distribution fitting for 35 months significant wave height data

It is assumed that the wave peak period (Tp) obeys conditional normal distribution for given Hs. The joint probability density function can be simulated a curved surface as shown in Figure C-2. Because the shape for this density function is irregular, we can hardly compute the probability for certain kind of combination of Hs and Tp by integration of this density function.

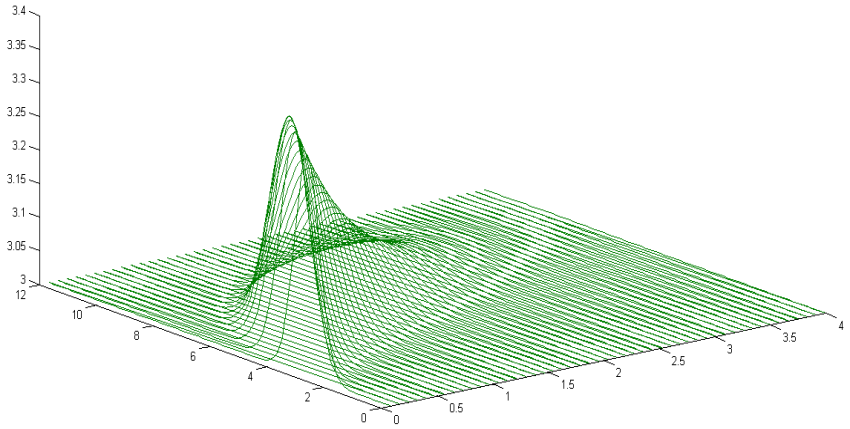

Figure C-2. Joint probability density function of Hs and Tp in 3-D coordinates

Therefore we try to use First-Order Reliability Method (FORM) mapping the variables Hs and Tp to a standard normal plane as two new variables U_1 and U_2.

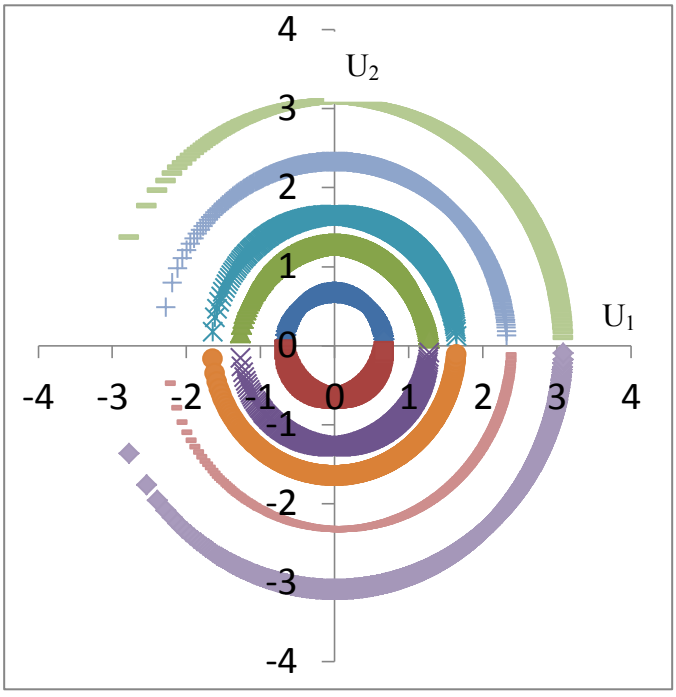

Figure C-3. Conformal mapping of Hs and Tp to standard normal U1-U2 Plane

Assuming Hs and Tp are independently distributed, we can compute their joint probability approximately by product of their own density function in terms of U_1 and U_2. For any given Hs and Joint Probability, we can thus obtain a unique U_2. Then, we can obtain the associated Hs and Tp by an inverse procedure.

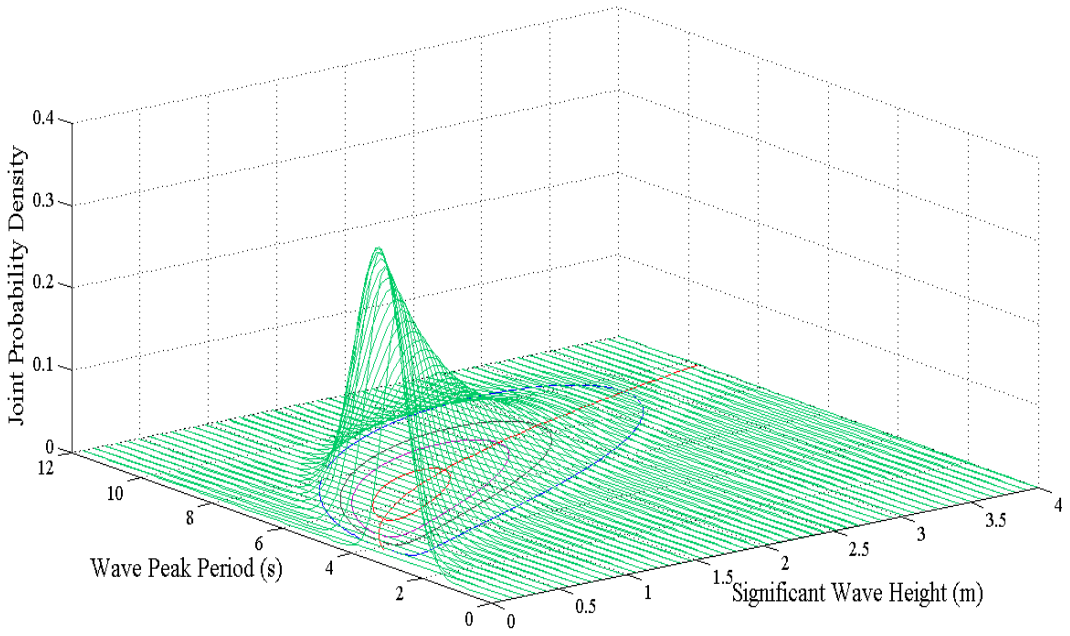

Figure C-4. The joint probability density function with Hs-Tp contour and regression line

VITA

Name: Lin Su

Address: Zachry Department of Civil Engineering
Texas A&M University
3136 TAMU
College Station, Texas 77843-3136
USA

Email Address: sulin1987@tamu.edu

Education: B.S., Hydropower and Water Conservancy Engineering, Hohai University, 2006